Mon. Not. R. Astron. Soc. **000**, ??–?? (2001) Printed 1 February 2008 (MN LaTeX style file v1.4)

The role of multipolar magnetic fields in pulsar magnetospheres

Estelle Asseo[1] and David Khechinashvili[1,2,3]
[1] *Centre de Physique Théorique, Ecole Polytechnique, 91128 Palaiseau CEDEX, France*
[2] *Institute of Astronomy, University of Zielona Góra, Lubuska 2, 65-265 Zielona Góra, Poland*
[3] *Center of Plasma Astrophysics, Abastumani Astrophysical Observatory, Al. Kazbegi Ave. 2a, 380060 Tbilisi, Georgia*

arXiv:astro-ph/0203129v3 19 Mar 2002

Received in original form

ABSTRACT
We explore the role of complex multipolar magnetic fields in determining physical processes near the surface of rotation powered pulsars. We model the actual magnetic field as the sum of global dipolar and star-centered multipolar fields. In configurations involving axially symmetric and uniform multipolar fields, 'neutral points' and 'neutral lines' exist close to the stellar surface. Also, the curvature radii of magnetic field lines near the stellar surface can never be smaller than the stellar radius, even for very high order multipoles. Consequently, such configurations are unable to provide an efficient pair creation process above pulsar polar caps, necessary for plasma mechanisms of generation of pulsar radiation. In configurations involving axially symmetric and non-uniform multipoles, the periphery of the pulsar polar cap becomes fragmented into symmetrically distributed narrow sub-regions where curvature radii of complex magnetic field lines are less than the radius of the star. The pair production process is only possible just above these 'favourable' sub-regions. As a result, the pair plasma flow is confined within narrow filaments regularly distributed around the margin of the open magnetic flux tube. Such a magnetic topology allows us to model the system of twenty isolated sub-beams observed in PSR $B0943+10$ by Deshpande & Rankin (1999, 2001). We suggest a physical mechanism for the generation of pulsar radio emission in the ensemble of finite sub-beams, based on specific instabilities. We propose an explanation for the subpulse drift phenomenon observed in some long-period pulsars.

Key words: pulsars: magnetic fields. plasmas: instabilities, waves.

1 INTRODUCTION

Observations and theory suggest that complex multipolar magnetic fields prevail near the surface of neutron stars, and play an important role in the physics of rotation powered pulsars.

The complexity of surface magnetic fields is determined by the evolution of magnetic fields in neutron stars. According to one scenario (e.g., Blandford, Applegate & Hernquist 1983), the magnetic field is generated by currents flowing in the thin outer crust of the star, with thickness $\Delta r \ll R_{\rm s}$, where $R_{\rm s} \approx 10^6$ cm is the neutron star radius. In this case, the superposition of magnetic multipoles of order $l \sim R_{\rm s}/\Delta r \geq 10$ dominates the exterior field (Arons 1993). Assuming that the evolution of magnetic fields in isolated neutron stars is due to ohmic decay, Mitra, Konar & Bhattacharya (1999) show that the evolution of such high-order multipolar components ($l \leq 25$) is very similar to that of the dipolar field: the structure of the pulsar surface field does not vary much as the pulsar ages. An alternative approach by Ruderman (1991a,b,c) attributes the surface magnetic field evolution to changes in the magnetic field present in the core. Due to stresses, caused by the spinning down or the spinning up of the neutron star, strong enough to drive the crustal lattice beyond its yield strength, moving magnetized crustal platelets are created and account for 'sunspot-like' clumps of magnetic field at the stellar surface.

One first reason for introducing non-dipolar magnetic fields close to the stellar surface lies in the inability for the pure surface dipolar field to provide sufficient pair production, as required for the generation of pulsar emission. In effect, in their classical paper, Ruderman & Sutherland (1975) state that the value of the radius of curvature of magnetic field lines, ρ, should be about $R_{\rm s} \approx 10^6$ cm near the stellar surface, in order to fulfill the conditions for a copious pair production process in the polar vacuum gap. However, such small curvature radii cannot be achieved assuming a pure dipolar magnetic field near the stellar surface: the contri-

© 2001 RAS

bution of non-dipolar magnetic components, present in the close vicinity of the neutron star in the form of either multipoles of order higher than the dipole one, or the 'sunspot-like' clumps, is necessary. These components are supposed to be strong enough to change the local topology of the magnetic field in the vicinity of pulsar polar caps. Arons & Scharlemann (1979) also point out that pair creation in pulsars with very long periods is impossible without invoking magnetic fields more complex than the dipolar one. In a thorough study of the space-charge limited flow of electrons in combined surface dipolar and quadrupolar magnetic fields, Barnard & Arons (1982) conclude that the curvature radii of resulting magnetic field lines can be much smaller than those of the pure dipolar field, and discuss the possible impact of this effect on both the pair creation process and the observations.

Chen & Ruderman (1993) specify the conditions for a sufficient pair production to be triggered off, as required for the generation of pulsar emission. They conclude that only a very twisted ($\rho_{\rm s} \sim R_{\rm s}$, where $\rho_{\rm s}$ is the curvature radius at the stellar surface) and strong ($B_{\rm s} = 2 \times 10^{13}$ G) magnetic field ensures that on the $P - \dot{P}$ diagram, the death line leaves all pulsars above itself, that is to say, 'permits' their existence. However, an exception is the recently discovered PSR J2144 $-$ 3933 with period $P = 8.5$ s (Young, Manchester & Johnston 1999), which appears to lie even below this death line. With this latter observation in mind, Gil & Mitra (2001) study anew the pair creation process in a super-strong magnetic field. They conclude that all observed pulsars, including PSR J2144 $-$ 3933, lie above the death lines deduced from their model, which adopts $B_{\rm s}/B_{\rm s}^{\rm d} \sim 100$ (although still $B_{\rm s} < B_{\rm q}$) and $\rho_{\rm s} \sim 0.1 R_{\rm s}$. Here, $B_{\rm q} \equiv m^2 c^3/e\hbar = 4.4 \times 10^{13}$ G is the critical magnetic field strength above which the photon splitting phenomenon may inhibit the pair formation process (Daugherty & Harding 1983), while $B_{\rm s}^{\rm d}$ and $B_{\rm s}$ are respectively the dipolar and the total - dipolar plus multipolar - magnetic field strengths at the stellar surface. Thus, according to Gil & Mitra (2001), such extremely strong and curved magnetic fields are able to resolve in a natural way the long-standing controversy about the so-called 'binding energy problem', from which vacuum gap models suffered so far, without the necessity to involve bare polar cap strange stars, as proposed by Xu, Qiao & Zhang (1999).

Unfortunately, only the dipolar component of the surface magnetic field, more exactly, only its component perpendicular to the line of sight, is inferred from the observed spin-down rate of a pulsar, thus leaving the possibility for different hypotheses. For instance, Krolik (1991) assumes that the rotational energy loss of a pulsar $I\Omega\dot{\Omega}$ results from the electromagnetic radiation generated by the ensemble of individual magnetic multipoles which are dominant at the pulsar light cylinder: this allows the surface value of each multipolar component to be constrained, so yielding limits on magnetic moments of high order; the tightest limits are obtained for millisecond pulsars, due to their short periods P and the small values of their derivatives $\dot{P}$. Such restrictions on high-order field strengths at the light cylinder do not necessarily mean their absence close to the stellar surface, where they can even play a dominant role. Krolik (1991) suggests that, if such is the case, the relative complexity of the profiles of millisecond pulsars results from the complexity of their actual magnetic field.

Recent interpretations of the observations of soft X-rays, probably emitted due to the heating of pulsar polar caps, lead to similar conclusions. Page & Sarmiento (1995, 1996) for instance, show that it is impossible to obtain the high level of observed pulsed fractions, or to describe asymmetric X-ray profiles, under the assumption of a purely dipolar field: a much better fit to the observations is obtained by including a suitably oriented quadrupolar field component. On the other hand, Cheng & Zhang (1999) in their model suggest that a strong and complex surface magnetic field significantly affects the two hard thermal components, usually present in the X-ray emission of pulsars.

Interest in a multipole field dominant close to the star goes back to Gil (1985), who introduced a dominant quadrupolar magnetic field in order to explain peculiarities in the radio emission of the millisecond PSR $1937 + 214$.

Recently observed features of radio emission of the pulsar PSR B0943+10, reported by Deshpande & Rankin (1999, 2001), clearly indicate the existence of a system of 20 rotating sub-beams, in circulation around the magnetic axis of the star. This well organized and stable pattern of emission has been observed at three different frequencies, namely at 430 MHz, 111.5 MHz (at Arecibo) and 34 MHz (in India), which are supposed to represent three different altitudes above the stellar surface, according to the Radhakrishnan & Cooke (1969) model. This system of emission sub-beams can be associated with a set of plasma columns, with their feet in the acceleration region. The relativistic pair plasma flow in these columns is guided by the strong dipolar magnetic field up to (and beyond) the altitudes corresponding to the radio emission generation region. At these altitudes, instabilities occurring in a particular plasma column give rise to a radio emission beam, independently of similar processes in adjacent columns. These beams form the emission cone. Deshpande & Rankin (2001) point out that the columns themselves are not drifting or rotating: it is the action in the acceleration region, located near the stellar surface, which is doing so while it feeds and maintains the plasma column just above it. Several processes in the individual sub-beams are found to be stable: circulation time, intensities, polarisation characteristics and dimensions. However, as noticed by Deshpande & Rankin (2001), there is no clear choice between a continuous drift effect and particle cascade sputters. They speculate that the memory of the sub-beam configuration may reside in either standing waves, or in heating of the surface (varying along the magnetic azimuth), or in the seeding of the plasma columns, for instance, by sparks, created on a non-integer multiple of the circumference and thus apparently drifting.

One way of describing successfully the observed set of discrete emission columns in the pulsar magnetosphere is to assume that close to the stellar surface the total magnetic field results from the superposition of a dipolar and a high-order multipolar components, both fields being axially symmetric and star-centered. Moreover, to fulfill the requirements for an efficient pair creation just above the surface of the star, namely the possibility to have at the stellar surface a very twisted total magnetic field, one may consider that the strength of the assumed multipolar magnetic field is higher than the dipolar field strength, or at least comparable to it, and test that the radius of curvature of resulting magnetic field lines is less than the stellar radius. This concerns the domain of open field lines, as the latter includes the region where the emission process is supposed to arise (at large distances from the stellar centre, $r \gg R_\mathrm{s}$). In this same domain, near the stellar surface, high magnetic multipolar components are supposed to be more efficient than the dipolar field in determining the properties of the vacuum gap and initiating the pair production process. Let us remark that by ‘vacuum gap‘ is meant the domain located just above the surface of the star in which a non-zero component of the electric field in the direction parallel to the background magnetic field is able to accelerate charges.

The likelihood of having a multipolar magnetic field with strength higher than, or comparable to the dipole field strength is reasonable if one takes into account the influence of the general-relativistic effect of inertial frame dragging on the electromagnetic field structure near a rotating neutron star, as suggested by Muslimov & Tsygan (1986). In Section 3.2 of this paper we estimate such amplification factors, using the formalism developed by Muslimov & Tsygan (1986), and confirm that these factors increase with the multipolar order l of the multipolar components involved. Therefore, the actual strength of the high-order multipolar field components near the stellar surface may appear to be much higher than those estimated in the flat space-time. On the other hand, as mentioned above, the evolution of multipolar magnetic fields with $l \leq 25$ due to ohmic diffusion follows the same pattern as that of the dipolar field (Mitra, Konar & Bhattacharya 1999). Therefore, there are reasonable grounds to believe that the dipolar and multipolar magnetic field components coexist and persist with their relative strengths.

The above configuration can be used to explore pulsar radio emission theories. For instance, the pulsar emission cone, when associated with a stable configuration of an ensemble of emission columns, could possibly be traced back to spark discharges in the pulsar polar gap region. This could be done in reference to recent works involving sparks and non-stationary plasma in vacuum gap models (Usov 1987; Ursov & Usov 1988; Asseo & Melikidze 1998; Melikidze, Gil & Pataraya 2000; Gil & Mitra 2001). In a different way, we model the whole system of observed twenty sub-beams as an ensemble of relativistic finite beams, flowing along the curved magnetic field lines of the open magnetosphere and immersed in external media. The two surrounding external media which limit these flowing sub-beams are, on one side, the medium that lies on closed field lines, and on the other side, the tenuous plasma present inside the hollow cone. The latter surrounds the pulsar magnetic axis, and is modified due to the presence of high-order multipolar magnetic field components near the stellar surface.

We show how, in the case of millisecond or fast pulsars, the geometrical characteristics of the flowing beams in the radial and azimuthal directions allow us to treat each beam of the ensemble as isolated and immersed in external media. The complex dispersion relation for perturbations of the system is simplified, as the beams are extremely thin and as the propagating waves are excited close to resonance in the radio domain. Such waves have simultaneously an electrostatic and electromagnetic character and thus are able to reach an observer. Depending on the distance of the considered region to the surface of the star, either the ’finite beam’, or the radiative, or the two-stream instability is the dominant one (Asseo 1995). Moreover, whatever the altitude and the concerned instability, unstable waves with characteristics in agreement with observed waves can be considered as candidates for pulsar radio emission. In particular, close to the surface of the star, above the gap region in which the observed beams are supposed to have their origin, the ’finite beam’ instability, dominant there, may initiate the radio emission process in the plasma columns. Farther away the classical emission processes are available.

In the case of slower pulsars, like PSR 0943+10, the geometrical characteristics of the flowing beams in the radial and azimuthal directions prevent considering each particular beam of the ensemble as isolated, just above the gap region and up to some distance $r_{2\mathrm{D}}$. There, all the beams forming the emitting region have to be treated simultaneously. This can be done by introducing the 3-dimensional dependence of the perturbed physical quantities, leading to a simple analytical treatment of the whole system of sub-beams. In between the gap region and the region located at and above $r_{2\mathrm{D}}$, simultaneous dependence of the perturbations on the radial and azimuthal variables will complicate the character of the emitted waves. In effect, the 3-dimensional character of perturbed physical quantities results in the coupling of the features of excited waves in the radial and azimuthal directions. Beyond the distance $r_{2\mathrm{D}}$, the sub-beams of the ensemble can be considered as isolated, so that the resulting perturbations should resemble those described above for fast pulsars: the character of the unstable emitted waves should be recovered. However, the existence of the necessary transition between the two regions, below and above $r_{2\mathrm{D}}$, and thus the required continuity of the wave-solutions through this transition zone, suggest the possibility for an apparent ’drift’ of the observed waves.

In the present paper we examine several magnetic configurations involving dipolar and strong multipolar magnetic field components, in order to determine those which provide small curvature radii, as required by standard magnetospheric models. Note that our calculations only concern the simplified case of the so-called aligned rotator, i.e. a pulsar whose dipolar magnetic momentum $\boldsymbol{\mu}$ is parallel, or anti-parallel, to the rotation axis $\boldsymbol{\Omega}$, and similarly for the magnetic momenta of the different multipoles. However, we believe that most of our qualitative results also apply to inclined rotators.

As a starting point we suppose that magnetic multipoles of order (l, m), created by the currents flowing in the stellar crust (Blandford et al. 1983; Arons 1993), are superimposed on the total dipolar field. A multipole component with $m = 0$ we refer to as ’axially symmetric and uniform’, and the one with a non-zero m – as ’axially symmetric and non-uniform’. Let us note that uniformity, and not the symmetry, is the main difference between these two structures of the magnetic field near the polar cap. Indeed, while $m = 0$ -type fields are simultaneously symmetric and uniform, $m \neq 0$ -type fields are symmetric around the magnetic axis but non-uniform, being fragmented as shown below. In Section 2, we present the general formalism to describe the multipolar fields. We also consider the configurations composed of the global dipolar field and a single axially symmetric and uniform multipolar field, and find out that ’neutral points' and 'neutral lines', i.e. places of zero magnetic field strength, may exist near the neutron star surface in such a geometry. In Section 3, we model the magnetic structure of complex configurations in the vicinity of the stellar surface, and calculate the curvature radii of resulting field lines near the stellar surface. We conclude that the curvature radii of field lines in configurations containing only axially symmetric and uniform multipolar fields are not small enough to ignite the pair creation process above the pulsar polar cap, even if contributing multipoles are of very high order. On the other hand, we find that configurations involving axially symmetric and non-uniform multipolar magnetic fields allow to achieve the small curvature radii of field lines, within a fraction of the modified polar cap. Furthermore, the pair plasma flow at large altitudes from the stellar surface appears to be fragmented into a system of isolated filaments, distributed symmetrically around the pulsar magnetic axis, around the margin of the open dipolar flux tube. We apply this model to PSR B0943 + 10 and find resemblance with the observed pattern of its radio emission (Deshpande & Rankin 1999, 2001). In Section 4, we discuss radio emission processes in the system of discrete sub-beams of dense plasma, surrounded by media of reduced density, in relation with an analysis previously proposed by Asseo (1995). This is done for either millisecond and fast pulsars or for slower pulsars like PSR B0943 + 10. A summary of our results is presented in Section 5.

2 MULTIPOLAR MAGNETIC FIELD COMPONENTS AROUND THE NEUTRON STAR

Throughout this paper we use a system of spherical coordinates (r, θ, ϕ) where r is the distance measured from the stellar centre, θ is the polar angle (in radians) measured from the z-axis, and ϕ is the azimuthal angle (in radians) measured from an arbitrary origin. The z-axis is directed along the dipolar momentum of the star $\boldsymbol{\mu}$.

2.1 General description of multipolar fields at close distances from the stellar surface

In the near zone limit ($kr \ll 1$), the magnetic field vector, $\boldsymbol{B}^{lm}(r,\theta,\phi)$, associated with a given magnetic multipole (lm), can be expressed in terms of spherical harmonics $Y_{lm}(\theta,\phi)$ (Jackson 1975):

$$\boldsymbol{B}^{lm}(r,\theta,\phi) = \nabla\left(\frac{Y_{lm}(\theta,\phi)}{r^{l+1}}\right). \tag{1}$$

Spherical harmonics are written in terms of the associated Legendre functions, as

$$Y_{lm}(\theta,\phi) = \sqrt{\frac{2l+1}{4\pi}\frac{(l-m)!}{(l+m)!}}P_l^m(\cos\theta)\,\mathrm{e}^{\mathrm{i}m\phi}, \tag{2}$$

where $P_l^m(x)$, the associated Legendre function, is defined as

$$P_l^m(x) = \frac{(-1)^m}{2^l l\,!}\left(1-x^2\right)^{m/2}\frac{\mathrm{d}^{l+m}}{\mathrm{d}x^{l+m}}\left(x^2-1\right)^l. \tag{3}$$

In a spherical geometry, the components of an individual multipolar magnetic field vector $\boldsymbol{B}^{lm}(r,\theta,\phi) = (B_r^{lm}(r,\theta,\phi), B_\theta^{lm}(r,\theta,\phi), B_\phi^{lm}(r,\theta,\phi))$ are written:

$$B_r^{lm}(r,\theta,\phi) = -4\pi\frac{l+1}{2l+1}\frac{q_{lm}}{r^{l+2}}Y_{lm}(\theta,\phi), \tag{4}$$

$$B_\theta^{lm}(r,\theta,\phi) = \frac{4\pi}{2l+1}\frac{q_{lm}}{r^{l+2}}Y_{lm}^{(1,0)}(\theta,\phi), \tag{5}$$

$$B_\phi^{lm}(r,\theta,\phi) = \frac{4\pi}{2l+1}\frac{q_{lm}}{r^{l+2}}\mathrm{i}m\sin\theta Y_{lm}(\theta,\phi). \tag{6}$$

Particular multipolar magnetic components are obtained for specific values of l and m, with $|m| \le l$. Namely, dipolar components are obtained for $l=1$ and either $m=0$ or $m=\pm1$, quadrupolar components for $l=2$ and either $m=0$, $m=\pm1$ or $m=\pm2$ and so on. If $m=0$ and l is arbitrary, then one obtains axially symmetric and uniform multipolar components.

The magnetic moment, associated with the strength of the magnetic multipole component (lm) at the surface of the star, is defined as $\mu^{lm} = B_{\mathrm{s}}^{lm}R_{\mathrm{s}}^{l+2}$.

The total magnetic field of the neutron star can be written as a sum of the individual multipolar magnetic field components. In the hypothesis where all the multipoles are centered at the centre of the star,

$$\boldsymbol{B}(r,\theta,\phi) = \sum_{l=1}^{\infty}\sum_{m=0,\pm1,\dots\pm l}\boldsymbol{B}^{lm}(r,\theta,\phi). \tag{7}$$

Magnetic field lines for the total magnetic field are obtained, as usual, from an integration of the set of differential equations:

$$\frac{\mathrm{d}r}{B_r(r,\theta,\phi)} = \frac{r\mathrm{d}\theta}{B_\theta(r,\theta,\phi)} = \frac{r\sin\theta\mathrm{d}\phi}{B_\phi(r,\theta,\phi)}. \tag{8}$$

A unit vector in the direction of the local magnetic field $\boldsymbol{B}(r,\theta,\phi)$ can be defined as:

$$\boldsymbol{b}(r,\theta,\phi) \equiv \frac{\boldsymbol{B}(r,\theta,\phi)}{B(r,\theta,\phi)}. \tag{9}$$

The absolute value of the derivative of $\boldsymbol{b}(r,\theta,\phi)$ along the field line is nothing else than the curvature of the magnetic field line. At a given point of space (r,θ,ϕ), the radius of curvature of the total magnetic field line is therefore defined as

$$\rho(r,\theta,\phi) = \frac{1}{|\left(\boldsymbol{b}(r,\theta,\phi)\nabla\right)\boldsymbol{b}(r,\theta,\phi)|}. \tag{10}$$

Naturally, if one assumes the existence of only one pure individual multipolar magnetic field component around the star, the equations of its field lines and their curvature radii can be easily obtained from equations (8) and (10) by substituting $\boldsymbol{B}^{lm}(r,\theta,\phi)$ instead of the total field $\boldsymbol{B}(r,\theta,\phi)$.

2.2 The case of axially symmetric and uniform multipolar magnetic fields: magnetic field components and the magnetic vector potential

In this section we treat multipolar magnetic fields of type $\boldsymbol{B}_{l0}$, i.e. those for which l is arbitrary but $m=0$. Such fields can be regarded to as 'dipolar-like', as they are axially symmetric and uniform in the vicinity of pulsar polar caps, like the dipolar magnetic field.

According to equations (4 − 7), for the case with $m = 0$, the components of the total magnetic field close to the surface of the star can be expressed in a general form as a sum of multipolar magnetic field components, namely

$$B_r(r,\theta) = \sum_{l=1}^{\infty} B_r^{l0}(r,\theta) =$$

$$\sum_{l=1}^{\infty} \frac{\mu^{l0}}{r^{l+2}}\, f^{l0}\left(\sum_{n=0}^{2n\leq l} c_{l-2n}\cos^{(l-2n)}\theta\right), \tag{11}$$

$$B_\theta(r,\theta) = \sum_{l=1}^{\infty} B_\theta^{l0}(r,\theta) =$$

$$\sum_{l=1}^{\infty} \frac{c^{l0}\mu^{l0}\sin\theta}{r^{l+2}}\, F^{l0}\left(\sum_{n=0}^{2n+1\leq l} c_{l-1-2n}\cos^{(l-1-2n)}\theta\right), \tag{12}$$

$$B_\phi(r,\theta) = \sum_{l=1}^{\infty} B_\phi^{l0}(r,\theta) = 0, \tag{13}$$

where $\mu^{l0} = B_{\rm s}^{l0} R_{\rm s}^{l+2}$ is the magnetic moment associated with $B_{\rm s}^{l0}$, the strength of the multipolar magnetic field component at the surface of the star, μ^{l0} being a positive quantity according to its definition; c^{l0} is a constant which depends on the order l of the multipole; f^{l0} and F^{l0} are specific functions which only depend on powers of $\cos\theta$; c_{l-2n} and c_{l-1-2n} are numerical coefficients.

As implied by Maxwell's equations, the static magnetic field vector can be defined through the magnetic vector potential $\boldsymbol{A}$, as $\boldsymbol{B} = (\nabla\times\boldsymbol{A})$. Thus, one can associate a vector potential $\boldsymbol{A}^{lm}$ with any arbitrary magnetic multipole with indices l and m. Obviously, in the axially symmetric and uniform case with arbitrary l and with $m = 0$, each multipolar component of the magnetic field vector, $\boldsymbol{B}^{l0}(r,\theta)$, derives from a potential vector $\boldsymbol{A}^{l0}(r,\theta)$. Assuming that the magnetic field is created by an extremely thin current that circulates all over the crust of the neutron star, the potential vector has only an azimuthal component $A_\phi(r,\theta)$, which can be specified for each particular magnetic multipole having indices $l \geq 1$ and $m = 0$, in terms of the corresponding current, or equivalently in terms of the magnetic moment μ^{l0} and the variables θ and r, as

$$A_\phi^{l0}(r,\theta) = \frac{\mu^{l0}\sin\theta}{r^{l+1}}\, F^{l0}\left(\sum_{n=0}^{2n+1\leq l} c_{l-1-2n}\cos^{(l-1-2n)}\theta\right), \tag{14}$$

where the functions F^{l0} have been introduced just above.

Magnetic field lines are obtained as usual from an integration of the set of two differential equations (8). Here, for the axially symmetric and uniform case with arbitrary l and $m = 0$, the ϕ-component of the magnetic field being zero, it is sufficient to consider the multipole magnetic field components in a plane $\phi = $ const, and to integrate only the first differential equation, namely

$$\frac{{\rm d}r}{B_r^{l0}(r,\theta)} = \frac{r{\rm d}\theta}{B_\theta^{l0}(r,\theta)}. \tag{15}$$

A systematic derivation of the equations of field lines of any particular magnetic multipole can also be obtained, introducing the function

$$\Psi^{l0}(r,\theta) \equiv r\sin\theta A_\phi^{l0}(r,\theta), \tag{16}$$

which is an integral of the field equations. Effectively, using the fact that magnetic field components of the multipolar magnetic field with indices ($l0$) derive from a vector potential $A_\phi^{l0}(r,\theta)$, we obtain:

$$B_r^{l0}(r,\theta) = \frac{1}{r\sin\theta}\frac{\partial}{\partial\theta}\left(A_\phi^{l0}(r,\theta)\sin\theta\right) = \frac{1}{r^2\sin\theta}\frac{\partial}{\partial\theta}\Psi^{l0}(r,\theta), \tag{17}$$

$$B_\theta^{l0}(r,\theta) = -\frac{1}{r}\frac{\partial}{\partial r}\left(rA_\phi^{l0}(r,\theta)\right) = -\frac{1}{r\sin\theta}\frac{\partial}{\partial r}\Psi^{l0}(r,\theta), \tag{18}$$

$$B_\phi^{l0}(r,\theta) = 0. \tag{19}$$

The function $\Psi^{l0}(r,\theta)$ is constant along a given field line; the behaviour of multipolar magnetic field components $B_r^{l0}(r,\theta)$ and $B_\theta^{l0}(r,\theta)$, necessarily follows the behaviour of the derivatives $\partial_r\Psi^{l0}(r,\theta)$ and $\partial_\theta\Psi^{l0}(r,\theta)$ along a given field line and in a given plane in which $\phi = $ const. As a consequence,

$$\Psi^{l0}(r,\theta) = {\rm const} \tag{20}$$

gives the general form for multipolar magnetic field line equations. For a magnetic multipole ($l0$), from equations (14) and (16), equation (20) can be written

$$\frac{\mu^{l0}\sin^2\theta}{r^l}\, F^{l0}\left(\sum_{n=0}^{2n+1\leq l} c_{l-1-2n}\cos^{(l-1-2n)}\theta\right) = {\rm const}. \tag{21}$$

The functions F^{l0} are very easily obtained for the successive multipolar components: $F^{10} = 1$, $F^{20} = \cos\theta$, $F^{30} = 3 + 5\cos 2\theta$, …, $F^{l0} = \sum_{n=0}^{2n+1\leq l} c_{l-1-2n}\cos{(l-1-2n)}\theta$, making use of the transformations of circular functions $F^{l0}\Big(\sum_{n=0}^{2n+1\leq l} c_{l-1-2n}\cos^{(l-1-2n)}\theta\Big) \equiv F^{l0}\Big(\sum_{n=0}^{2n+1\leq l} c'_{l-1-2n}\cos{(l-1-2n)}\theta\Big)$. These functions, according to equation (21), provide magnetic field line equations for the appropriate particular multipolar fields. Drawing of the field lines in a plane where $\phi = $ const, shows that a pure magnetic multipole of order l makes $2l$ loops around the centre of the star.

A function $\Psi(r,\theta)$ can be associated with the total magnetic field: considering that the total magnetic field, in a given plane $\phi = $ const, is the sum of the successive multipolar magnetic field components, the function $\Psi(r,\theta)$ is the sum of the successive functions $\Psi^{l0}(r,\theta)$ defined above. The general form of the function $\Psi(r,\theta)$ can be written

$$\Psi(r,\theta) = \sum_{l=1}^{\infty}\Psi^{l0}(r,\theta) = r\sin\theta\sum_{l=1}^{\infty}A_\phi^{l0}(r,\theta). \tag{22}$$

Consequently, the total function $\Psi(r,\theta)$, written as an infinite sum,

$$\Psi(r,\theta) = \sin^2\theta\sum_{l=1}^{\infty}\frac{\mu^{l0}}{r^l}\, F^{l0}\left(\sum_{n=0}^{2n+1\leq l} c_{l-1-2n}\cos^{(l-1-2n)}\theta\right), \tag{23}$$

provides the total magnetic field line equation $\Psi(r,\theta) = $ const in the given plane $\phi = $ const.

Using the specific contributions of the first multipoles, together with the functions F^{l0} introduced in equation (12) (see also the text below equation 21), and with the adequate numerical coefficients, we have:

$$\Psi(r,\theta) = \sin^2\theta \left[\frac{\mu^{10}}{r} + \frac{\mu^{20}}{r^2}\cos\theta + \frac{\mu^{30}}{r^3}(3 + 5\cos 2\theta) + \ldots \right.$$
$$\left. + \frac{\mu^{l0}}{r^l}\, F^{l0}\left(\sum_{n=0}^{2n+1\leq l} c'_{l-1-2n} \cos{(l-1-2n)\theta} \right) + \ldots \right]. \quad (24)$$

2.3 The case of axially symmetric and uniform multipolar magnetic fields: neutral lines, neutral points

The surface $\Psi(r,\theta) = 0$ separates field lines with opposite direction, that is field lines on which the magnetic field has reversals. Whatever the number of multipoles, the function $\Psi(r,\theta)$ is zero for either $\theta = 0$, or $\theta = \pi$, or when the variables r and θ are such that $\sum_{l=1}^{\infty} Y_{l0}^{(1,0)}(\theta,\phi) = 0$. Obviously, there should be some particular relation between the magnetic moments μ^{l0} to have $\Psi(r,\theta) = 0$, and thus a total magnetic field with zero strength, $B(r,\theta) = 0$, in any arbitrary plane $\phi = \mathrm{const}$ and at some point (r,θ), as, for instance, at the surface of the star, where $r = R_\mathrm{s}$.

Values of the magnetic field on the lines $\theta = 0$, or $\theta = \pi$ are easily obtained. From the equations (11) – (13), giving the magnetic field components, it is clear that on the lines $\theta = 0$ and $\theta = \pi$, $B_\phi(r,\theta) = 0$, as it is zero everywhere, $B_\theta(r,\theta) = 0$, since $\sin\theta$ is in factor, but $B_r(r,\theta)$ takes-on values that depend on the particular point where the radial component of the multipolar magnetic field is calculated. In particular, on the line $\theta = \pi$, there is a point at which $B_r(r,\theta) = 0$. A study of the behaviour of the magnetic field around this point will probably show that it may be considered as a neutral point for particular configurations of the magnetic field in the pulsar magnetosphere. For instance, this should be the case when the total magnetic field can be represented by a combination of either dipolar and quadrupolar magnetic fields, or dipolar and octupolar magnetic field, or dipolar and 16-polar magnetic field and so on, the equations for the field lines being, respectively,

$$\Psi(r,\theta) = \sin^2\theta \left(\frac{\mu^{10}}{r} + \frac{\mu^{20}}{r^2}\cos\theta \right), \quad (25)$$

$$\Psi(r,\theta) = \sin^2\theta \left(\frac{\mu^{10}}{r} + \frac{\mu^{30}}{r^3}(3 + 5\cos 2\theta) \right), \quad (26)$$

$$\Psi(r,\theta) = \sin^2\theta \left(\frac{\mu^{10}}{r} + \frac{\mu^{40}}{r^4}(9\cos\theta + 7\cos 3\theta) \right), \quad (27)$$

and so on.

On the side of the pole where $\theta = 0$, there is no real solution for r, the r-solutions being either negative or imaginary. By contrast, on the side of the other pole, where $\theta = \pi$, there is a point r at which the magnetic field strength is zero, and changes sign around this point. Effectively, for the combination of a dipole plus a multipole of even order ($l = 2n, n = 1, 2, \ldots$), there is a point where the strength of the magnetic field is zero. The solution $r_\mathrm{np}^{l1} = (\text{numerical coefficient}) \left(B_\mathrm{s}^{l0}/B_\mathrm{s}^{10}\right)^{1/(l-1)} R_\mathrm{s}$, depends on the ratio of the multipolar and the dipolar magnetic field strengths. More generally, for an arbitrary θ-angle there is a neutral line on which the magnetic field is zero. For instance, if the magnetic field is taken as the simple combination of dipolar and quadrupolar magnetic fields, the function

$$\Psi(r,\theta) = \sin^2\theta \left(\frac{\mu^{10}}{r} + \frac{\mu^{20}}{r^2}\cos\theta \right) \quad (28)$$

becomes zero at either $\theta = 0$ or $\theta = \pi$, or on the line where

$$\frac{\mu^{10}}{r} + \frac{\mu^{20}}{r^2}\cos\theta = 0, \quad (29)$$

that is to say, on the circle defined by the equation

$$\cos\theta = -r\frac{\mu^{10}}{\mu^{20}} = -\frac{r}{R_\mathrm{s}}\frac{B_\mathrm{s}^{10}}{B_\mathrm{s}^{20}}. \quad (30)$$

In this case, there are three neutral lines: the two axes, $\theta = 0$ and $\theta = \pi$ and a circle in the plane (r,θ), on which the only acceptable r-solutions correspond to θ-angles in the domain $[\pi/2, 3\pi/2]$. Indeed, depending on the respective values of μ_{10} and μ_{20}, the r-solutions on the neutral circle have a physical meaning, or none. As an example, for the combination of dipolar and quadrupolar magnetic fields, the 'neutral point' is located at distances from the centre of the star $r_\mathrm{np}^{21} = 1.16 \left(B_\mathrm{s}^{20}/B_\mathrm{s}^{10}\right) R_\mathrm{s}$. On this line $\theta = \pi$, B_r is positive at smaller distances, $r < r_\mathrm{np}^{21}$, and negative at larger distances, $r > r_\mathrm{np}^{21}$. The 'neutral point' is located at the surface of the star only if B_s^{20} is less than B_s^{10}, so that $B_\mathrm{s}^{20} = B_\mathrm{s}^{10}/1.16 = 0.86 B_\mathrm{s}^{10}$.

As clear from the general results given above, similar locations for the 'neutral points' can be easily obtained for any combination of a dipolar field plus a multipolar field with an even index l. A study of the behaviour of the magnetic field on lines close to the 'neutral line' is necessary to conclude about the specific physical processes in this region.

3 MODELLING THE MAGNETIC FIELD STRUCTURE NEAR THE STELLAR SURFACE: TOPOLOGY OF POSSIBLE CONFIGURATIONS AND CURVATURE RADII OF FIELD LINES

3.1 General description of the method of calculation

In this section we study the topology of magnetic field configurations near the stellar surface, which consist of a multipolar magnetic field $\boldsymbol{B}^{lm}$ (with $l > 1$ and $|m| \leq l$), superimposed on the global dipolar field of the pulsar $\boldsymbol{B}^\mathrm{d} \equiv \boldsymbol{B}^{10}$. We also introduce the ratio of the total and the dipolar magnetic field strengths,

$$\beta(r,\theta,\phi) \equiv \frac{B(r,\theta,\phi)}{B^\mathrm{d}(r,\theta,\phi)}, \quad (31)$$

where $B(r,\theta,\phi) \equiv |\boldsymbol{B}^\mathrm{d}(r,\theta,\phi) + \boldsymbol{B}^{lm}(r,\theta,\phi)|$. Therefore, $\beta(r,\theta,\phi)$ indicates how many times the strength of the total field exceeds the strength of its dipolar component, at a given point of space (r,θ,ϕ). In the calculations reported in Sections 3.3 and 3.4, particular attention is paid to the cases where the curvature radius of magnetic field lines at the stellar surface is smaller than the stellar radius, i.e. $\rho_\mathrm{s} \leq R_\mathrm{s}$, at least within a fraction of the modified polar cap. Intuitively, one would expect that such configurations assume a significant contribution of the multipolar component, so that $\beta_\mathrm{s} \equiv \beta(R_\mathrm{s},\theta,\phi) > 1$.

In order to test various magnetic configurations, we redefine the expression for the multipolar field components (equation 1) by introducing an extra amplification factor ξ as a free parameter, so that this expression now takes the following form:

$$\boldsymbol{B}_{lm}(r,\theta,\phi) = \xi\nabla\left(\frac{Y_{lm}(\theta,\phi)}{r^{l+1}}\right). \tag{32}$$

A specific choice of the ξ-factor in every particular example considered below, is justified by the output: it should allow us to obtain the expected structure and strength of the surface magnetic field above the modified polar cap. Amplification of certain multipolar components is discussed in detail in Section 3.2.

In order to model the geometry of the total magnetic field, one has to solve the set of differential equations (8), which is now convenient to rewrite in the following form:

$$r\frac{\mathrm{d}\theta(r)}{\mathrm{d}r} = \frac{B_\theta\left(r,\theta(r),\phi(r)\right)}{B_r\left(r,\theta(r),\phi(r)\right)}, \tag{33}$$

$$r\sin\theta(r)\frac{\mathrm{d}\phi(r)}{\mathrm{d}r} = \frac{B_\phi\left(r,\theta(r),\phi(r)\right)}{B_r\left(r,\theta(r),\phi(r)\right)}. \tag{34}$$

This set of equations has to be solved for the unknown functions $\theta(r)$ and $\phi(r)$.

Of course, the complex surface magnetic field should transform into the global pure dipolar field at large altitudes from the stellar surface, where multipolar components effectively vanish. This is warranted by the choice of correct boundary conditions while solving the set of equations (33) – (34). Since the generation of radio emission is associated with the bundle of the open dipolar magnetic field lines (i.e. those crossing the light cylinder), we restrict our calculations to this domain of the magnetosphere.

Let us introduce some distance $r_{\rm i}$, where surface fields are negligibly small, $B^{lm}(r_{\rm i},\theta(r_{\rm i}),\phi(r_{\rm i})) \ll B^{\rm d}(r_{\rm i},\theta(r_{\rm i}),\phi(r_{\rm i}))$, so that the total magnetic field can be treated as purely dipolar there. At this distance, the points of the last dipolar open field lines delineate a certain circle, and their azimuthal angle $\phi(r_{\rm i})$ takes arbitrary values within the range $0 \le \phi(r_{\rm i}) \le 2\pi$. According to the equation for the dipolar field lines,

$$\frac{r}{\sin^2\theta} = \mathrm{const}, \tag{35}$$

the polar angle of these points can be written

$$\theta_{\rm i} = \arcsin\sqrt{\frac{r_{\rm i}}{R_{\rm LC}}} \approx \arcsin\left(1.45\times10^{-2}P^{-0.5}\sqrt{\frac{r_{\rm i}}{R_{\rm s}}}\right). \tag{36}$$

Here $R_{\rm LC} = Pc/2\pi$ is the light cylinder radius of the pulsar, and P is the pulsar period. The dipolar field falls off with the distance as $(R_{\rm s}/r)^3$, whereas the multipolar field of order l falls off as $(R_{\rm s}/r)^{l+2}$, according to equations (4) – (6). Therefore, using equation (31), the characteristic distance $r_{\rm B}$, where $B^{lm} \sim B^{\rm d}$, can roughly be estimated as

$$r_{\rm B} \sim (\beta_{\rm s}-1)^{1/(l-1)}R_{\rm s}. \tag{37}$$

Thus, the dipolar field dominates over the multipolar field in the domain of altitudes $r \gg r_{\rm B}$ (and vice versa). Choice of $r_{\rm i}$ in the latter domain warrants a smooth transition from the complex surface field to the open dipolar field lines. Hence, this is equivalent to the integration of the field line equations from the stellar surface up to the light cylinder.

As well-known, observations of pulsar radio emission and most of the models for its generation imply that it originates at altitudes $r \ge 50R_{\rm s}$. Interpretation of radio observations indicates that the magnetic field is purely dipolar in the generation region, so that complex surface fields should vanish at such altitudes*. In other words, the complex surface field lines should connect to pure dipolar field lines well below $r = 50R_{\rm s}$. We verify that this requirement is fulfilled through out our calculations, for each chosen ξ-parameter.

Hence, the boundary conditions at $r = r_{\rm i}$ for different field lines are to be taken within the following angular range:

$$0 \le \theta(r_{\rm i}) \le \theta_{\rm i},$$
$$0 \le \phi(r_{\rm i}) \le 2\pi. \tag{38}$$

Each set of boundary conditions defines a single open field line, starting at the stellar surface, where the multipolar magnetic field dominates over the dipolar field, and extending to the domain located at altitudes $r \ge r_{\rm i}$ where the field is purely dipolar and axially symmetric and uniform. We use a Fehlberg fourth-fifth order Runge-Kutta method (see, e. g., Forsythe et al. 1977) in order to obtain the numerical solutions of the set of equations (33) – (34).

The results of our simulations are presented in the following subsections. We separate them into two cases, which have diverse physical consequences, namely: i) configurations composed of axially symmetric and uniform multipolar magnetic fields with $m = 0$ and the global dipolar field, and ii) configurations composed of axially symmetric and non-uniform multipolar fields with $m \ne 0$ and the global dipolar field. Before starting to discuss these particular cases, let us present one of the arguments in favour of an anomalous amplification of the 'weight' of multipolar components at the stellar surface, with respect to the dipole field.

3.2 Intensification of multipolar magnetic field components due to the general relativistic effect of inertial frame dragging

As mentioned in Section 1, high-order multipolar fields may be intensified close to the surface of a rotating neutron star, relatively to their value in a flat space, due to the general-relativistic effect of inertial frame dragging studied by Muslimov & Tsygan (1986). The exterior gravitational field of a neutron star, rotating with a constant angular velocity Ω, is described by the metric, which is locally inertial at the infinity:

$$\mathrm{d}s^2 = g_{\alpha\beta}\mathrm{d}x^\alpha\mathrm{d}x^\beta, \quad \alpha,\beta = 0,1,2,3. \tag{39}$$

The nonzero components of the metric tensor are written as follows:

$$g_{00} = -g_{11} = 1 - \frac{R_{\rm g}}{r}, \; g_{22} = -r^2,$$
$$g_{33} = -r^2\sin^2\theta, \; g_{03} = \frac{2GJ}{c^3r}\sin^2\theta. \tag{40}$$

---

* Although, the anomalous dispersion measure of the high-frequency versus low-frequency radio pulses, observed in some pulsars (Davies et al. 1984; Kuzmin 1992), has been attributed to the presence of the quadrupolar component of the magnetic field in the emission region.

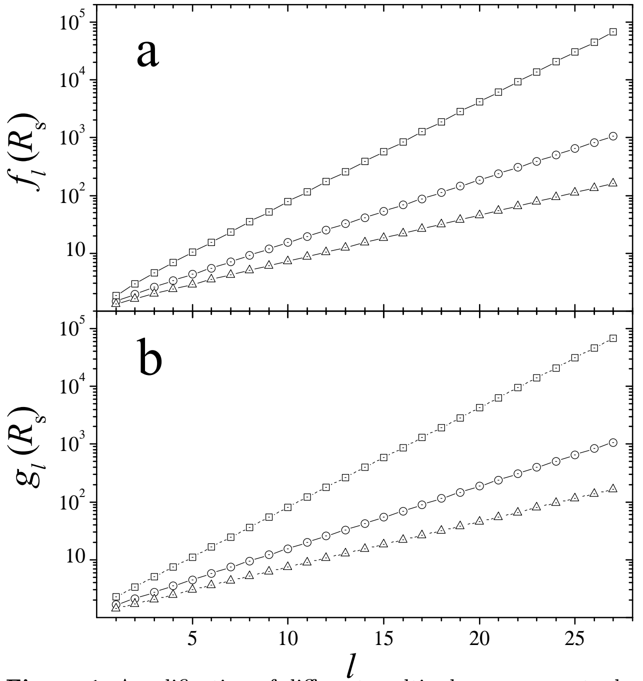

Figure 1. Amplification of different multipolar components due to the frame dragging effect (equations 45 and 46). The values of the functions $f_l(r)$ and $\sqrt{g_{00}}g_l(r)$ at the stellar surface ($r = R_{\rm s}$), given by equations (43) and (44), are plotted versus l in panels (a) and (b), respectively. This plot corresponds to the neutron star with the presumed mass $M = 1.4M_\odot$. The curves with squares, circles and triangles represent the calculations for the presumed stellar radii of 7×10^5 cm, 10^6 cm and 1.3×10^6 cm, respectively.

Here $R_{\rm g} = 2GM/c^2$ is the Schwarzschild radius, G is the gravitational constant, c is the speed of light, M is the mass of the neutron star and J is its angular momentum.

Muslimov & Tsygan (1986) solved the Maxwell equations in such a geometry, and found the modified magnetic field components modified as follows:

$$\tilde{B}_r(r,\theta,\phi) = \sum_{lm} (l+1) \left(\frac{R_{\rm s}}{r}\right)^{l+2} f_l(r)\; b_{lm}\, Y_{lm}(\theta,\lambda), \tag{41}$$

$$\tilde{B}_{\theta,\phi}(r,\theta,\phi) = \sum_{lm} \left(\frac{R_{\rm s}}{r}\right)^{l+2} \sqrt{g_{00}} g_l(r)\; b_{lm}\, \nabla_{\theta,\phi} Y_{lm}(\theta,\lambda). \tag{42}$$

Here b_{lm} are some coefficients defined from the boundary conditions (see equations 4 – 6), $\lambda = \phi - \Omega t$, and the functions $f_l(r)$ and $g_l(r)$ can be expressed in terms of hypergeometric functions,

$$f_l(r) = F\left(l, l+2; 2(l+1); \frac{R_{\rm g}}{r}\right), \tag{43}$$

$$g_l(r) = F\left(l+1, l+2; 2(l+1); \frac{R_{\rm g}}{r}\right). \tag{44}$$

Therefore, the modified radial and angular multipolar magnetic field components are connected with the corresponding components in the flat space, as

$$\tilde{B}_r^{lm} = f_l(r) B_r^{lm}, \tag{45}$$

$$\tilde{B}_{\theta,\phi}^{lm} = \sqrt{g_{00}} g_l(r) B_{\theta,\phi}^{lm}. \tag{46}$$

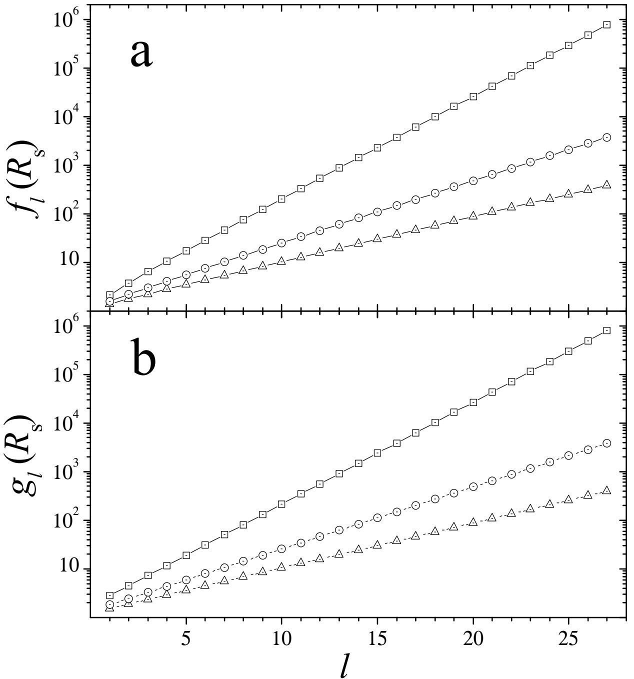

Figure 2. The same as in the previous figure, but for the neutron star with the presumed mass $M = 1.6M_\odot$.

Estimates of the values of the functions $f_l(r)$ and $\sqrt{g_{00}}g_l(r)$ at the stellar surface, $r = R_{\rm s}$, are displayed in Figs. 1 and 2, for a presumed mass of the neutron star $M = 1.4M_\odot$ and $M = 1.6M_\odot$, respectively. The functions $f_l(r)$ and $g_l(r)$ are calculated for three different cases of the model neutron star radii, namely $R_{\rm s} = 7 \times 10^5$ cm, 10^6 cm and 1.3×10^6 cm. First, one notices that the resulting intensification is about the same for the radial and angular magnetic field components, and is stronger for the higher-order multipoles. Second, multipolar fields are amplified more intensively near the surface of relatively smaller and more massive neutron stars. Indeed, according to Fig. 2, high-order multipolar magnetic field components with $l \leq 25$ in the curved space may be even $10^4 - 10^5$ stronger than the corresponding components in the flat space.

The evolution with time of multipolar magnetic field strengths in isolated neutron stars has been studied by Mitra et al. (1999), assuming that the field is mostly generated in the outer crust of the star and its later evolution is due to the ohmic decay of currents in the crustal layers. They have shown that if one assumes the same initial strength for all multipolar magnetic fields, the evolution is such that the reduction with time is similar to that of the dipole field component, except for very high multipole orders ($l > 25$).

A combination of the two described effects, that is, the intensification of multipolar magnetic field components due to general relativistic effects and evolution with time of their strengths, suggests that multipolar magnetic field components with high order should be present at the surface of neutron stars and important enough to determine the magnetic configuration in their vicinity. This justifies the choice of ξ (equation 32) as a free parameter in our calculations below.

3.3 Complex configurations containing axially symmetric and uniform multipolar magnetic fields: field line topology and curvature radii

In this section we present the results of our calculations for the magnetic configurations composed of the global dipolar field and a surface multipolar field with $m = 0$ and arbitrary $l \geq 1$. As mentioned in the beginning of Section 2.2, such fields can be regarded as 'dipolar-like', as they are axially symmetric and uniform in the vicinity of pulsar polar caps. Due to this fact, the ratio of the total and the dipolar magnetic field strengths at the stellar surface, $\beta_{\rm s}$ (equation 31), is independent of the azimuth ϕ and also almost independent of the polar angle θ, within the modified polar cap of a pulsar. It should be noticed that the polar cap still has a circular shape, as in the pure dipolar case. However, as a result of magnetic flux conservation, the presence of a strong surface magnetic field with $\beta_{\rm s} > 1$ reduces its angular radius to $\theta_p^{l0} = \theta_p^{\rm d}\beta_{\rm s}^{-0.5}$, compared to that of the pure dipolar polar cap, $\theta_p^{\rm d} \approx 1.45 \times 10^{-2} P^{-0.5}$ [rad].

For pure multipolar magnetic field lines with $m = 0$ (i.e., in the absence of the dipolar component), a first-order approximation for the curvature radius is obtained from equation (10), as

$$\rho^{l0} \approx \frac{4}{l(l+2)}\frac{r}{\theta}. \qquad (47)$$

For example, the curvature radius of the last open field lines at the stellar surface ($r = R_{\rm s}, \theta = \theta_p^{l0}$) for a pure multipole ($l0$) is:

$$\rho_{\rm s}^{l0} \approx \frac{276\ \beta_{\rm s}^{0.5} P^{0.5}}{l(l+2)} R_{\rm s}. \qquad (48)$$

However, as demonstrated below, the presence of the dipolar magnetic field in the actual configuration near the stellar surface modifies the values given by equation (48), especially assuming small and moderate values of $\beta_{\rm s}$.

As an example, we consider a sample pulsar with $P = 0.2$ s and $\dot{P} = 10^{-15}$ s/s. The surface dipolar magnetic field of such a pulsar is estimated as $B_{\rm s}^{\rm d} \approx 3.2 \times 10^{19} \left(P\dot{P}\right)^{0.5} \approx 4.4 \times 10^{11}$ G. Such a value allows intensification of the surface field up to 100 times, without exceeding the critical field $B_{\rm q} = 4.4 \times 10^{13}$ G. We model the dipole plus single multipole magnetic field lines of this pulsar, according to the scheme described in Section 3.1, and calculate the curvature radii of the last open field lines at the stellar surface. Our aim is to check how strong should be the contribution of axially symmetric and uniform multipolar components near the stellar surface, in order to achieve the desired small values of curvature radii of the resulting open magnetic field lines, as required for an efficient pair creation process.

The curvature radii of the last open field lines at the stellar surface are presented in Figs. 3(a), (b) and (c), which correspond to cases where the total surface magnetic field exceeds the dipolar component 2, 10 and 100 times, respectively. The solid lines with circles represent the results of our numerical calculations for given complex configurations. The dotted lines with triangles show, for comparison, what would be the curvature radii of the involved multipolar magnetic field lines in the absence of the dipolar field (as given by equation 48).

In Fig. 3(a) it is seen that, if the contribution of surface multipolar fields is comparable to the dipolar one, $\beta_{\rm s} = 2$, the radius of curvature of resulting field lines remains larger than the stellar radius, $\rho_{\rm s} > R_{\rm s}$, even for multipolar fields of very high order, $l \geq 25$. On the other hand, the dotted line shows that, in the absence of the dipolar field, $\rho_{\rm s} \leq R_{\rm s}$ would be achieved already for multipoles with $l \geq 12$. Therefore in this case, multipolar fields are simply too weak to 'twist' the field lines strongly enough.

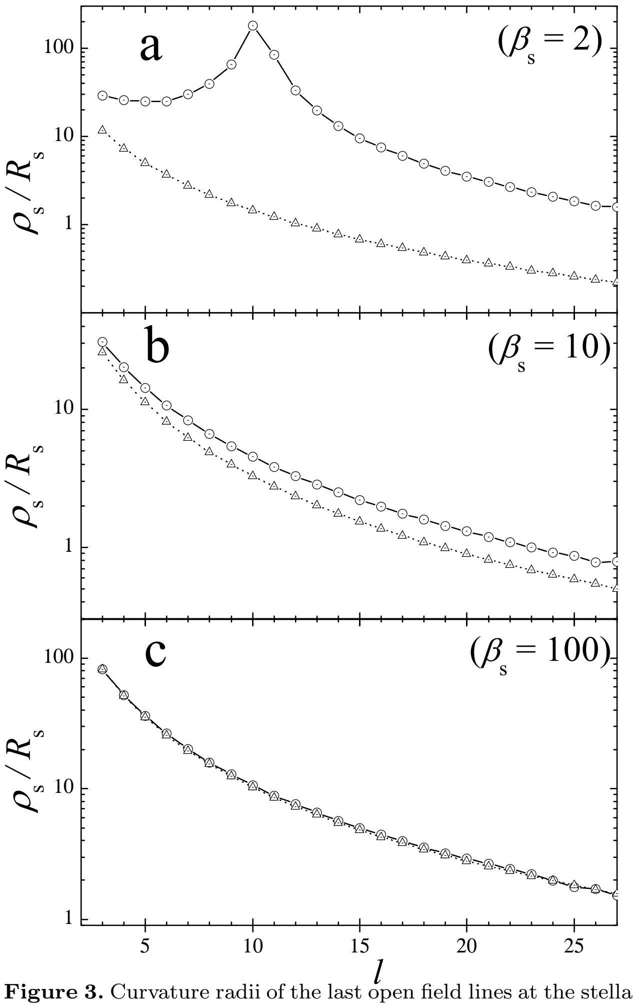

Figure 3. Curvature radii of the last open field lines at the stellar surface in the configurations composed of the global dipolar field and the axially symmetric and uniform multipolar field with $m = 0$, as functions of the multipolar order l. The three panels (a), (b) and (c) correspond to the three different cases of relative contribution of the multipolar components to the surface field strength, $\beta_{\rm s} = 2$, $\beta_{\rm s} = 10$ and $\beta_{\rm s} = 100$, respectively. The solid lines with circles correspond to the calculations for the complex surface field, whereas the dotted lines with triangles represent curvature radii, as they would be in the absence of the dipolar field (equation 48).

The situation is somewhat better, if one assumes a stronger contribution of multipolar fields, $\beta_{\rm s} = 10$. This case is presented in Fig. 3(b). As seen in this figure, the curvature radii of field lines become less than the stellar radius, if the multipolar order of contributing multipoles is very high, $l \geq 24$, still quite a possible case, according to Mitra et al. (1999).

However, a further increase of the contribution of surface multipolar fields worsens the situation. For instance, in the case of $\beta_{\rm s} = 100$, presented in Fig. 3(c), curvature radii never drop below the stellar radius, even when very high-order multipolar components ($l \geq 25$) contribute into the total magnetic field. This fact is easy to explain: such strong multipoles fully determine the surface field structure near the stellar surface. Indeed, the dotted line in Fig. 3(c), corresponding to the absence of the dipolar component, almost follows the solid line, corresponding to the total surface magnetic field. On the other hand, the high surface field strength leads to a highly (10 times) reduced angular radius of the polar cap, which, according to equation (48), provides larger curvature radii.

Therefore, we conclude that in the configurations composed of the global dipolar field and the axially symmetric and uniform multipolar fields, the curvature radii of the open field lines do not generally have curvature radii, small enough to fulfill the conditions for a copious pair creation process. At the same time, as seen in Fig. 3(c), in the configurations composed of global dipole and axially symmetric and uniform multipole, it is impossible to have both $\rho_{\rm s} \leq R_{\rm s}$ and $\beta_{\rm s} \sim 100$ in the same configuration, as implied by the vacuum gap model of Gil & Mitra (2001). These conclusions are true at least for multipolar fields of order $l \leq 25$, which do not significantly dissipate during the pulsar characteristic life-time (Mitra et al. 1999).

3.4 Complex configurations containing axially symmetric and non-uniform multipolar magnetic fields: field line topology and curvature radii

Let us now study magnetic field configurations composed of a global dipolar field on which non-axisymmetric multipolar magnetic fields (i.e. those with $m \neq 0$) are superimposed. We again restrict our calculations to the open magnetic flux tube. As in the previous section, we start our calculations at some altitude $r_{\rm i}$ where $B^{lm}(r_{\rm i}, \theta, \phi) \ll B^{\rm d}(r_{\rm i}, \theta, \phi)$, and solve the set of equations (33) and (34) from $r_{\rm i}$ down to the stellar surface. While doing so, we take the boundary conditions in the range (38). This allows us to find the footprints of the tube of open field lines on the stellar surface, i.e., to construct the modified polar cap. Our aim is to get solutions which provide $\rho \leq R_{\rm s}$ at the stellar surface, at least within a fraction of the modified polar cap, which is necessary for an efficient pair production process. We adjust the free parameter ξ (introduced in equation 32) in each particular case considered below, in order to obtain desired configurations. Throughout our calculations we control the value of the total surface magnetic field, so that it does not exceed $B_{\rm q}$ within the polar cap. Obviously, there is a great variety of possible configurations. Here we present the most illustrative ones. Let us first make a few general remarks.

A pure multipolar magnetic field (l, m) with $m \neq 0$ has $2m(l - m + 1)$ poles over the whole stellar surface. Out of those, along each latitude containing poles, $2m$ poles of alternating polarity are distributed around the axis of symmetry. At a given latitude, each pole with a given polarity is neighboured on its sides by two poles of the opposite polarity. The inclusion of the global dipolar field changes this topology. In effect, the dipolar field lines which enter one of the two polar regions on the stellar surface, are only able to connect to the local multipolar poles of a given polarity, and not to the poles of the opposite polarity. This reduces to m the number of local poles, which are close to each of the polar regions. One expects that the influence of these local multipolar poles is stronger at the annular edge of the polar cap. Consequently, the polar cap becomes modified: its edge becomes rather fragmented into m independent 'hot spots', as demonstrated below.

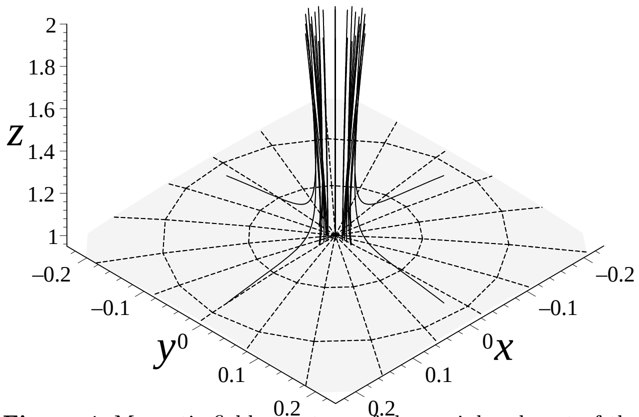

Figure 4. Magnetic field structure of the peripheral part of the open flux tube near the stellar surface, corresponding to the mixture of the dipolar field and the multipole of order $l = 4$ and $m = 4$. The Cartesian coordinates x, y and z are represented in the units of the stellar radius $R_{\rm s}$.

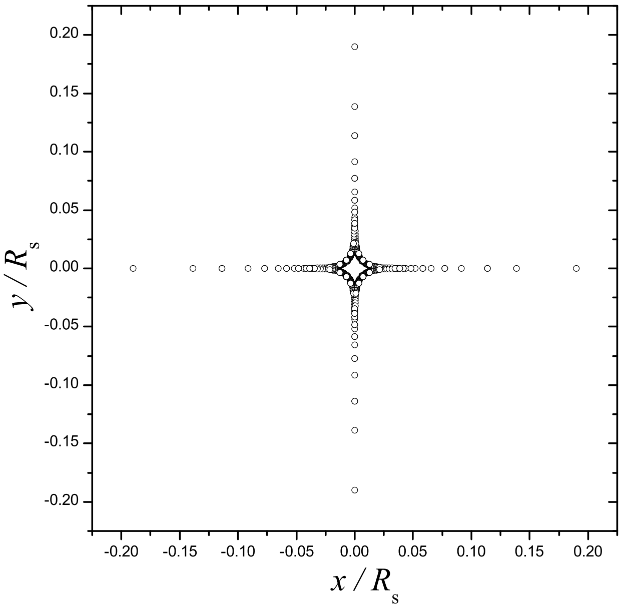

Figure 5. Peripheral fraction of the modified polar cap for the contributing multipole $l = 4, m = 4$. The footprints of the open field lines are represented by circles. Deformation of the polar cap under the influence of the local multipolar poles is clearly seen.

The most interesting cases, in our opinion, are those where the maximum number of local poles surround the magnetic z-axis of symmetry of the dipolar field at the closest angular distance, i.e. those with $l = m$. As an example, let us first consider the multipolar magnetic field with $l = 4$ and $m = 4$, superimposed on the global dipolar field.

The open field line geometry for such a configuration near the stellar surface and the corresponding modified polar cap (composed of the footprints of the open field lines) are presented in Figs. 4 and 5, respectively. The calculations were done for a sample pulsar with $P = 1$ s and $\dot{P} = 10^{-15}$ s/s. For simplicity, we only present in these figures the outermost 0.2 fraction of the open flux tube and its projection at the stellar surface (the inner, more central open field lines are less affected by the multipolar field, and follow rather the dipolar pattern). In other words, the boundary conditions at an altitude $r_{\rm i} = 10R_{\rm s}$ (see equations 36 and 38) were taken within the following angular ranges:

$$0 \leq \phi(r_{\rm i}) \leq 2\pi, \quad 0.8\theta_{\rm i} \leq \theta(r_{\rm i}) \leq \theta_{\rm i}. \tag{49}$$

Each of these ranges was divided into a fixed number of equal parts, both by the azimuth and the polar angle, so that the angular spacings between the initial points at the altitude $r_{\rm i}$ were taken equal.

Fig. 4 shows that the bundle of last open field lines, which is circumferentially uniform at higher altitudes, $r \geq 2R_{\rm s}$, where the multipolar magnetic field is negligible, tends to be deformed under the influence of the multipolar field closer to the stellar surface. As it is also seen in Fig. 5, the field lines are most significantly deviated outwards in those ϕ-directions, where the poles with an appropriate polarity are located. On the contrary, in the directions towards the multipolar poles of the opposite polarity, field lines deviate inwards from the pure dipolar circular pattern. The resulting polar cap appears to be rather distorted, as displayed in Fig. 5.

One would expect that both the magnetic field strength and the curvature radius of the field lines also vary within the periphery of the modified polar cap, so that both of them now appear to be functions of θ and ϕ, as opposed to the configurations containing axially symmetric and uniform multipolar components (discussed in Section 3.3), where both $\beta_{\rm s}$ and $\rho_{\rm s}$ could be treated as constant throughout the modified polar cap. Let us study this dependence.

Fig. 6(a) displays the azimuthal variation of $\beta_{\rm s}$ (i.e., the value of the total surface magnetic field normalized to the local value of the dipolar component) at the feet of the last open field lines. Fig. 6(b) displays the same total magnetic field measured in the units of the critical field $B_{\rm q}$. An apparent increase of the magnetic field is seen in the direction of the appropriate multipolar poles, whereas the field retains its almost dipolar strength in between these peaks (the minimum field strength is achieved towards the multipolar poles of the opposite polarity). In Fig. 6(b) we see that the field may increase to a significant fraction of $B_{\rm q}$ on certain field lines.

Fig. 6(c) shows the azimuthal variation of the curvature radius (derived from equation 10) of the last open field lines at the stellar surface. Clearly, $\rho_{\rm s} \sim (0.1 \div 1)R_{\rm s}$ only for the group of field lines stretched in the direction of the multipolar poles, whereas the surface value of the curvature radius of the remaining field lines (directed rather to opposite poles) is much larger than the stellar radius. The same conclusion would follow from an intuitive analysis of Fig. 4, where it is seen that the multipolar poles of an ’appropriate’ polarity tend to bend the field lines in their direction, thus to increase their curvature. On the contrary, the opposite poles ’repel’ and thus straighten the field lines directed to them.

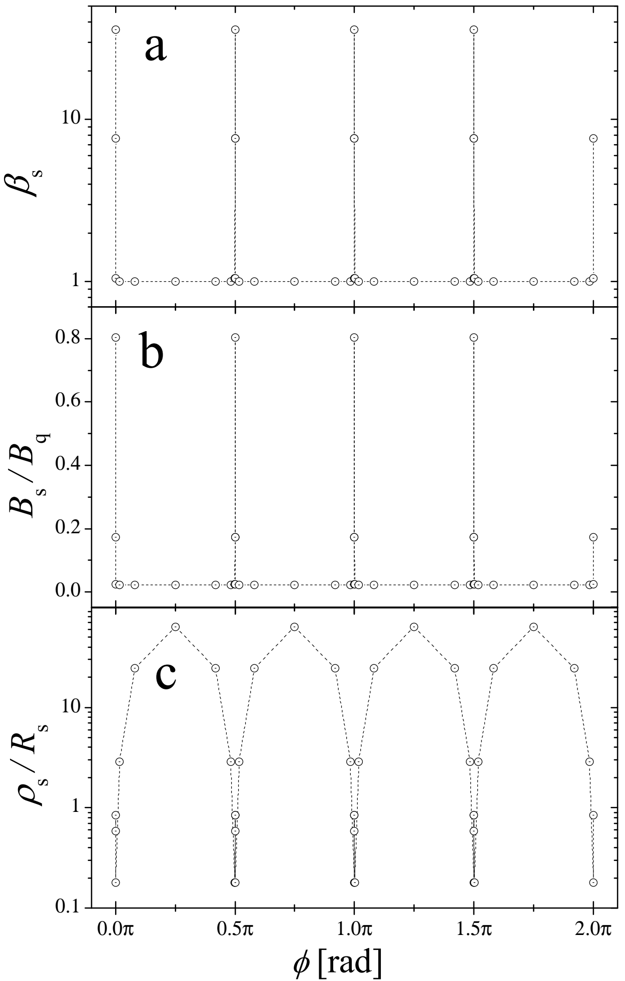

Figure 6. Dependence of $\beta_{\rm s}$, $B_{\rm s}/B_{\rm q}$ and $\rho_{\rm s}$ on the azimuthal angle ϕ, at the feet of the last open field lines, for the contributing multipole $l = 4, m = 4$. Conditions for pair creation are only fulfilled in localised regions, where $\rho_{\rm s} \leq R_{\rm s}$.

Dependence of $\beta_{\rm s}$, $B_{\rm s}/B_{\rm q}$ and $\rho_{\rm s}$ on the polar angle θ in the direction of an ’appropriate’ multipolar pole is displayed in Figs. 7(a), (b) and (c), respectively. These figures show that $\beta_{\rm s} \geq 1$ and $\rho_{\rm s} \sim (0.1 \div 1)R_{\rm s}$ at the peripheral fraction of the polar cap. At the same time, as we have seen in Figs. 6(a), (b) and (c), the polar cap periphery is also modulated azimuthally.

Therefore, it can be concluded that the conditions for a copious pair creation process are only fulfilled in localized regions, symmetrically distributed around the dipolar magnetic axis, within the thin peripheral part of the modified polar cap. Although at high altitudes above the stellar surface the field lines strictly follow the dipolar geometry, which is azimuthally uniform, such a non-uniform pattern of plasma creation near the stellar surface is to be reflected in the non-uniformity of the secondary plasma density distribution within the cross-section of the open magnetic flux tube at some large altitude ($r \geq r_{\rm i}$). First of all, the pair plasma will only flow along the outermost narrow conical layer of the open dipolar flux tube. The radial θ-width of this layer can be estimated from Fig. 7(c). Indeed, out of

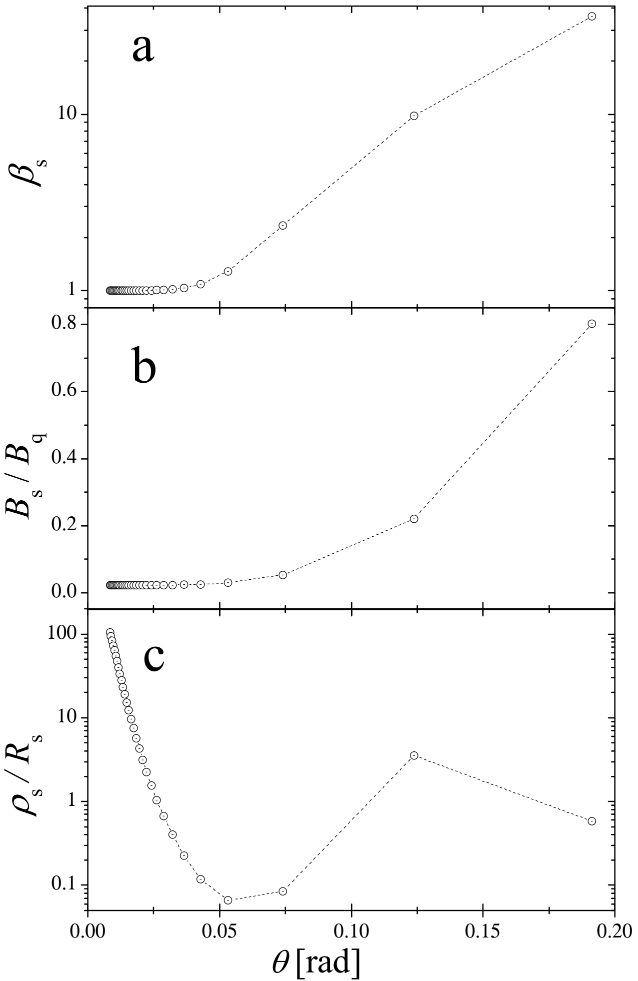

Figure 7. Dependence of $\beta_{\rm s}$, $B_{\rm s}/B_{\rm q}$ and $\rho_{\rm s}$ on the polar angle θ, in the direction of the local multipolar pole of order $l = 4, m = 4$.

the 30 footprints of the open field lines displayed in this figure, only outermost 10 of them are feet of the field lines with $\rho_{\rm s} \sim (0.1 \div 1) R_{\rm s}$. Recalling that these points have equal spacing at large altitudes and also taking into account the boundary conditions (49), one can estimate that the width of the conical layer loaded by the pair plasma will constitute about $(1 - 0.8)/3 \approx 0.07$ fraction of the total angular radius of the open flux tube. Moreover, this flow will also be fragmented azimuthally: pair plasma will flow only along the bundles of field lines which were stretched towards the local multipolar poles while emerging from the stellar surface. In the case of $l = 4, m = 4$, presented above, this corresponds to four isolated bundles of field lines. Therefore, plasma flow will be confined into a thin 'patchy hollow cone'. On the other hand, it is well known that physical processes leading to the generation of pulsar radio emission are associated with the existence of a dense pair plasma. That being so, the resulting emission cone will appear as split into symmetrically distributed 'hot spots'. This is how, in our opinion, the 'memory' of the surface field structure is preserved in the pulsar radio emission beam.

Let us notice that such a geometry is able to provide azimuthally localized emission beams in both the vacuum gap model (Ruderman & Sutherland 1975) and its competing space charge limited flow model (Arons & Scharlemann 1979, modified by Muslimov & Tsygan 1992). As well-known, the latter model has previously been criticized mainly because of its inability to provide isolated plasma filaments and associated beams of emission. The inclusion of multipolar magnetic fields with $m \neq 0$ removes the necessity of introducing spark discharges above the polar cap, as complex surface fields directly fragment the flow into isolated plasma columns.

3.5 Complex configurations containing axially symmetric and non-uniform multipolar magnetic fields: a model for PSR B0943 + 10

A study of field line topology and determination of curvature radii in a configuration involving a multipole of high-order is proposed with intent to interpret the special radio emission features observed for PSR B0943+10, whose dynamical parameters are: $P = 1.0977$ s and $\dot{P} = 3.529 \times 10^{-15}$ s/s. We assume that, for some reason, the open magnetic flux tube near the surface of this pulsar is only dominated by the global dipolar field plus the multipolar magnetic field with $l = 20$ and $m = 20$, an assumption which agrees with the results of Mitra et al. (1999).

The calculations according to the same scheme as in the previous case were done for the field lines which, at the initial height $r_{\rm i} = 1.5 R_{\rm s}$ (where $B_{20,20} \ll B_d$), constitute the outermost 0.1 fraction of the open field lines tube. In other words, the boundary conditions were taken within the following range:

$$0.9\theta_{\rm i} \leq \theta(r_{\rm i}) \leq \theta_{\rm i}, \qquad (50)$$
$$0 \leq \phi(r_{\rm i}) \leq 2\pi.$$

Let us notice that, just like in the previous case, angular spacings between the initial points within these ranges at the distance $r_{\rm i}$ were taken equal, both in azimuth ϕ and in polar angle θ.

The magnetic field structure of such a configuration near the stellar surface is presented in Fig. 8. Similarly to the previous case, we observe that some field lines deviate outwards, that is, towards the 'appropriate' local multipolar poles, whereas other field lines deviate inwards. For clearness, we again do not represent in this plot (and the other figures below) the inner open field lines, which are less affected by the multipolar field, and hence follow the dipolar geometry.

Fig. 9 represents the peripheral part of the modified polar cap of this pulsar. It is clearly seen that the outer margin of the polar cap appears to be fragmented into 20 symmetrically arranged sub-regions. One such particular sub-region is plotted in detail in Fig. 10. The azimuthal variation of the total magnetic field strength measured in the units of, first, the dipolar field, and then, the critical field, as well as the variation of the curvature radius of the last open field lines within this sub-region are displayed in Figs. 11(a), (b) and (c), respectively. The variation of $\beta_{\rm s}$, $B_{\rm s}/B_{\rm q}$ and $\rho_{\rm s}$ with the polar angle θ towards an 'appropriate' multipolar pole within this sub-region is presented in Figs. 12(a), (b) and (c), respectively. It is seen in these figures that the conditions for the development of pair cascades are fulfilled only above the restricted areas of the polar cap periphery.

At large altitudes from the stellar surface, the 'memory'

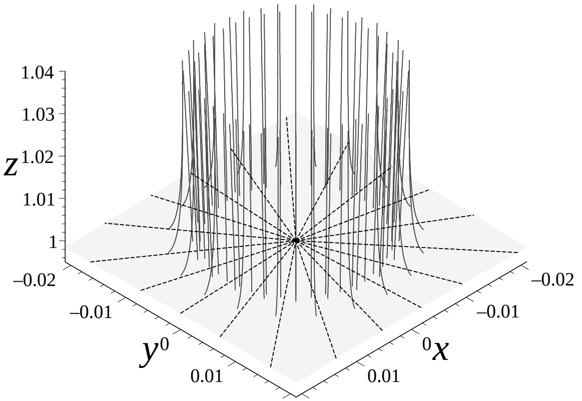

Figure 8. Magnetic field structure of the peripheral 0.1 fraction of the open flux tube near the surface of PSR B0943+10, assuming that the magnetic field is composed of the dipolar field and the multipole of order $l = 20$ and $m = 20$.

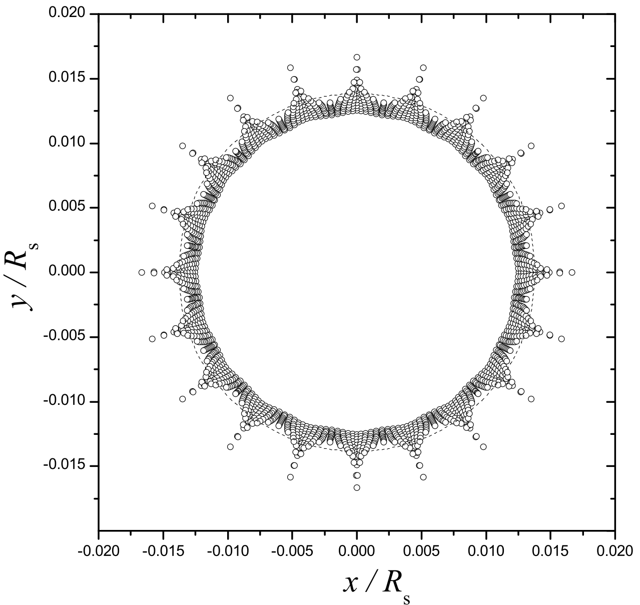

Figure 9. Peripheral fraction of the modified polar cap of PSR B0943 + 10 assuming the contribution of the multipolar component with $l = 20, m = 20$. The footprints of the open field lines are represented by circles. The dashed circle shows, for comparison, the margin of the corresponding purely dipolar polar cap.

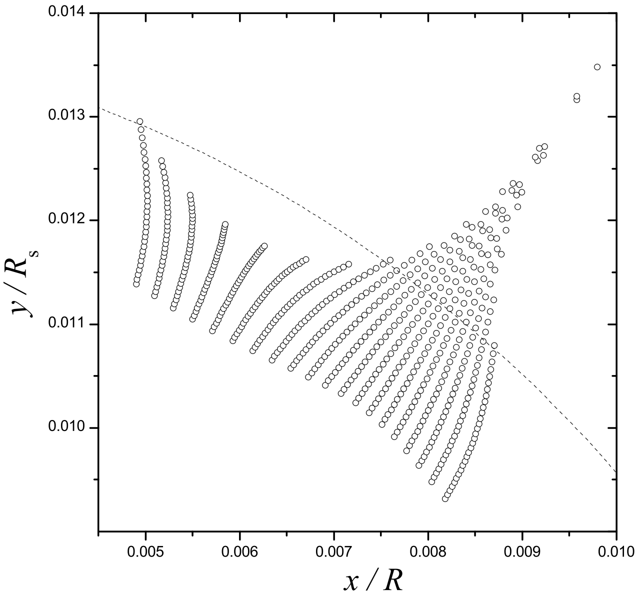

Figure 10. A fraction of the modified polar cap (see Fig. 9), representing one of the localized sub-regions where the curvature radius of the open field lines varies from 'favourable' to 'unfavourable' values for the pair creation process.

of the surface field structure will be preserved in the form of localized plasma columns distributed symmetrically around the outer margin of the open magnetic flux tube. Similarly to the previous case of $l = 4$ and $m = 4$, the radial width of this thin outer ring can be estimated from Fig. 12(c), using the boundary conditions (51): it will constitute about 1/20 fraction of the total radius of the open field lines tube. This 'hollow cone' will also be fragmented azimuthally, and the transverse dimension of an individual plasma column can be estimated from Fig. 11(c) as being about 1/40 fraction of the circumference. These plasma columns will be separated by low-density 'slits' of approximately the same transverse angular dimension.

Obviously, such a structure of the open flux tube exhibits a striking similarity with the 20-fold pattern of emission sub-beams discovered by Deshpande & Rankin (1999, 2001) using their 'cartographic transformation' technique. They found an identical configuration at two different frequencies, which suggests a filamentary plasma distribution rather than an emission process, as a possible origin for such a pattern. Deshpande & Rankin (2001) conclude that such plasma columns should have feet within a certain ring on the polar cap. In view of our multipolar model, such a ring could be associated with the outer margin of the modified polar cap, represented in Fig. 9.

According to Deshpande & Rankin (1999), 20 emission sub-beams undergo rigid counter-clockwise rotation around the magnetic axis in a total time of $37P = 41$ s, maintaining their number and spacing despite perturbations tending both to bifurcate a given beam and to merge adjacent ones. Although at this stage it is only possible to speculate about several possible reasons for this effect, we suggest in the next section an explanation of such a rotation, in terms of the character of the perturbations in the azimuthal direction.

In another way, such a phenomenon could actually reflect some stroboscopic-like effect. Indeed, pair creation in one of the sub-regions in Fig. 9 results in a roughly Gaussian distribution of the pair plasma density across the local magnetic field. Such a distribution function would screen the electric field, at least partially, in the adjacent sub-regions, thus temporarily ceasing or, at least, largely reducing the pair production process there. The situation would revert after pair plasma cascade will exhaust in this sub-region, when the accelerating electric field is screened out. Then, two adjacent sub-regions will 'turn on', reducing pair creation in their adjacent sub-regions. Such consecutive 'switches', in combination with the $\boldsymbol{E} \times \boldsymbol{B}$-drift and the polar cap heating, may result in the above-mentioned stroboscopic effect.

It should be noticed that, in order to obtain the patterns presented in Figs. 9 − 12, one has to choose the free

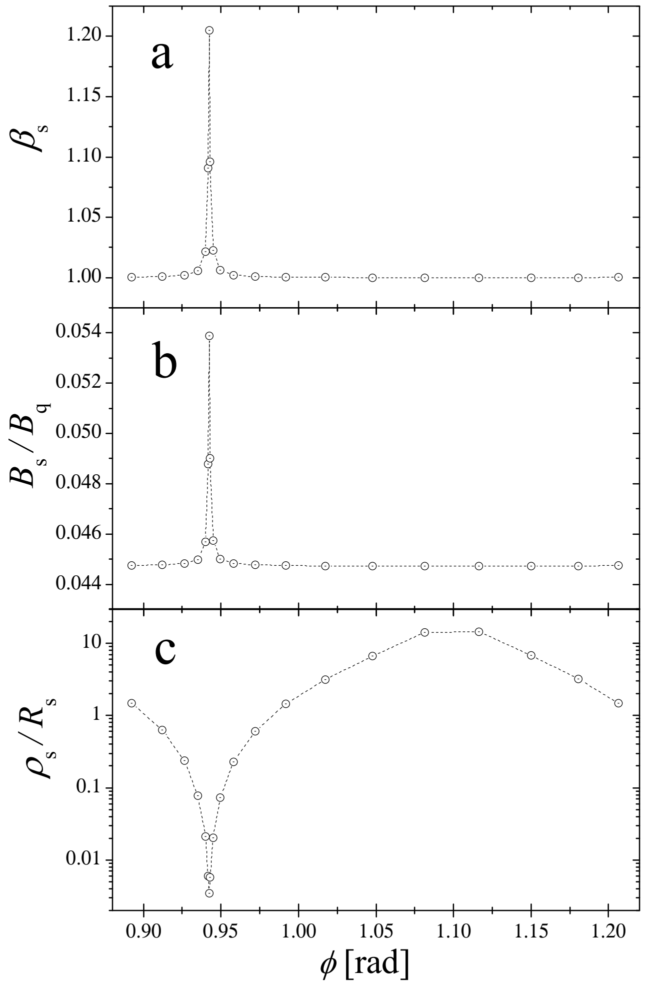

Figure 11. Dependence of β_s, B_s/B_q and ρ_s on the azimuthal angle ϕ, at the feet of the last open field lines of PSR B0943 + 10, assuming contribution of the multipole $l = 20, m = 20$.

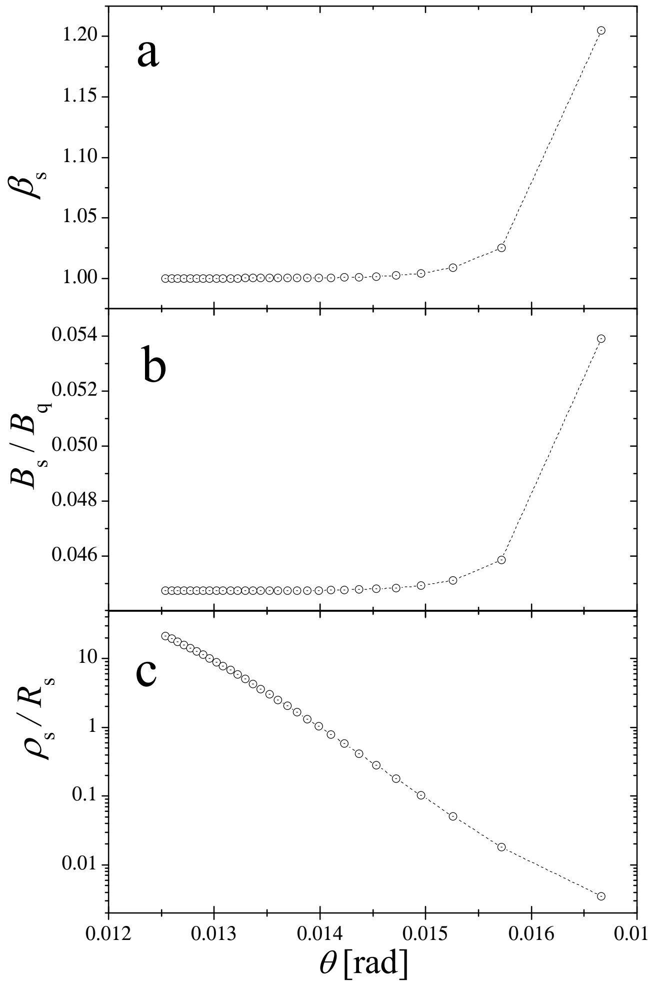

Figure 12. Dependence of β_s, B_s/B_q and ρ_s on the polar angle θ, in the direction of the local multipolar pole, for the same pulsar.

parameter ξ (introduced in equation 32) in our calculations so that the magnetic field strength in the close vicinity of the multipolar poles themselves appears to exceed significantly the critical field B_q. However, these multipolar poles are located at lower latitudes of the stellar surface, close to the neutron star's equator. Therefore, very high magnetic field is achieved well within the domain of the closed field lines where plasma creation processes certainly do not occur. Besides, there are no serious theoretical limitations to the strength of the magnetic field in nature (Usov V. V., private communication).

4 A MODEL FOR RADIO EMISSION FROM AN ENSEMBLE OF FINITE SUB-BEAMS

4.1 Features of the model

As demonstrated in Section 3.4, the particular magnetic field topology which results from the superposition of the global dipolar magnetic field and a high-order multipolar field with $m \neq 0$, both with high strength, suggests that the pair plasma created at the bases of magnetic flux tubes is guided within isolated thin filaments, located at the outer margin of the bundle of open magnetic field lines. According to Sturrock (1971), the density of the pair plasma within the flux tubes is proportional to the Goldreich & Julian (1969) density, namely $n_p = \kappa n_{GJ}$, the κ parameter being in the domain $10^3 \leq \kappa \leq 10^5$. Outside, the plasma is supposed to have a much smaller density, of the order of the Goldreich & Julian density, n_{GJ}. Thus, the whole system of dense filaments can be described as an ensemble of relativistic finite beams immersed in external low-density media. These external media in the pulsar magnetosphere are, on the one hand, the charged static medium lying on closed field lines, and on the other hand, the primary beam formed of ultra-relativistic particles of one charge flowing inside the hollow cone and between the dense beams.

The simplest case concerns one flowing annular beam of relativistic pair plasma surrounded by external plasmas. The dispersion relation giving the characteristics of perturbations able to propagate in such a system were obtained matching the solutions for the electromagnetic field components at the different beam-plasma interfaces (Asseo 1995). The case of the ensemble of twenty isolated sub-beams discussed in Section 3.5 is more complex: the beams are supposed to be regularly distributed over a ring that delimits the emission region; they have different radial and azimuthal extents and are separated over the ring by distances of the order of their azimuthal extent. The radial variation of the density operates in two different ways: either there is an abrupt change of the density at the edges of the ring, or there is none. The azimuthal changes of the density from one beam to the next one are alike. The geometrical characteristics of the relativistic beams are evaluated taking into account the fact that the observed ensemble of twenty beams have their origin in the gap region, very close to the stellar surface, where the complex multipolar field determines the pair creation process. As concluded in the previous section (see Figs. 12(c) and 11(c) for details), the radial angular width of an individual sub-beam constitutes a fraction equal to about 1/20 of the total radius of the open field lines tube at an altitude $r_{\rm i}$ (where $B^{lm} \ll B^{\rm d}$), whereas its azimuthal angular width represents a fraction equal to about 1/40 of the circumference. Therefore, at some distance $r_{\rm i}$ (see Section 3.1), the radial and azimuthal extents of individual sub-beams can be estimated as, respectively,

$$w_\theta = \frac{r_{\rm i} \sin\theta_{\rm i}}{20} \approx 7.3 \times 10^2 P^{-1/2} \left(\frac{r_{\rm i}}{R_{\rm s}}\right)^{3/2} \; [\rm cm] \tag{51}$$

and

$$w_\phi = \frac{2\pi r_{\rm i} \sin\theta_{\rm i}}{40} \approx 2.3 \times 10^3 P^{-1/2} \left(\frac{r_{\rm i}}{R_{\rm s}}\right)^{3/2} \; [\rm cm], \tag{52}$$

where equation (36) has been used in order to evaluate $\theta_{\rm i}$. For example, at a distance $r_{\rm i} = 2R_{\rm s}$, far above the gap region, the numerical estimates for the individual sub-beam width yield $w_\theta \approx 2 \times 10^3$ cm and $w_\phi \approx 6.5 \times 10^3$ cm, respectively, for a pulsar with period $P = 1$ s. The ratio of the azimuthal and radial sub-beam widths is constant, namely $w_\phi/w_\theta \approx \pi$ whatever the distance, but the typical wavelengths associated with observed radio frequencies are smaller than these characteristic widths. Thus, one should test whether it is sufficient to consider two-dimensional perturbations of the whole system of beams immersed in exterior media, or if it is necessary to analyse the fate of 3-dimensional perturbations. This can be checked as in Asseo, Pellat & Sol (1983), considering the strongest instabilities which may develop in a thin beam surrounded by different plasmas.

In the previous sections we used the spherical system of coordinates (r, θ, ϕ), centered at the stellar centre. Instead, in this section it is convenient to use a cylindrical system of coordinates (ϱ, φ, z), adequate for a local description. Here the radial coordinate ϱ is measured along the local curvature radius of the magnetic field line; φ is the azimuthal angle which corresponds to the angular variation along the circle with the radius ρ, this circle being tangent to the magnetic field line passing through the point (r, θ) in the plane $\phi = \phi_0$ of the spherical geometry; z is the coordinate perpendicular to the plane $\phi = \phi_0$.

Assuming 3-dimensional perturbations in the cylindrical system depending on (ϱ, φ, z) and characterized by wavenumbers m and k_z, the strongest instabilities are obtained at the resonant frequency $\omega \approx mc/\rho$ and for transverse wavenumbers in the domain $\Delta k_z \leq \sqrt{2} m^{2/3} \rho^{-1}$. In this case the analytical solutions obtained for the electromagnetic fields characterizing the perturbation in terms of Bessel and Hankel functions, result in an unmodified growth rate of the instabilities. Consequently, they are valid for beams with a spatial extent

$$\Delta z = w_\phi \geq \Delta z_{\rm min} \equiv \sqrt{2} \pi m^{-2/3} \rho, \tag{53}$$

where we used the fact that the spatial extent of a sub-beam $\Delta z = 2\pi/\Delta k_z$ is nothing else but its azimuthal width w_ϕ (equation 52).

4.2 The case of millisecond and fast pulsars

Numerical estimates show that in the case of millisecond and fast pulsars the constraint (53) is easily fulfilled just above the gap region and beyond, considering the domain of observed radio frequencies $\nu = 2\pi/\omega$ (see Figs. 13(a) and (b), respectively). This indicates that in such a case, finite transverse dimensions do not modify the results obtained in cylindrical geometry using two-dimensional perturbations to characterize radio emission features generated above the gap region within an annular hollow conical beam, or within an ensemble of discrete sub-beams similar to those observed in PSR B0943 + 10.

In such conditions, one may consider that locally the propagating wave only sees the radial variations of the density, so that it is possible to treat the problem in a poloidal plane. While doing so, we ignore the density variations in the direction corresponding to the azimuthal ϕ-direction of the spherical geometry, that is to say, in the transverse z-direction of the cylindrical geometry, and treat each beam of the ensemble of beams as isolated and immersed in 'infinite' exterior media. This allows us to extend the results which concern the characteristics of the perturbations able to propagate in the system formed by relativistic beam and plasma flows which fill a hollow conical region and are immersed in exterior media, to the more complex situation of the ensemble of beams.

The dispersion relation specific to the case of a finite beam immersed in external media was obtained by matching the solutions for the electromagnetic field components at the different beam-plasma interfaces (Asseo 1995). It can be expressed in terms of the dielectric constant for the relativistic beam plus relativistic plasma flows, W, and of the dielectric constants of the exterior media, W_i and W_e. It is obtained close to the resonant frequency,

$$\omega \approx m\Omega_0 + \delta\omega \approx \omega_{\rm R} + \delta\omega \approx \omega_{\rm R}(1 + Y), \tag{54}$$

where $m\Omega_0 \approx mc/\rho$ is the frequency associated with the circulation of relativistic particles along magnetic flux tubes and $Y = \delta\omega/\omega_{\rm R} \leq 1$ is the relative growth rate. Assuming variations with the radial distance together with a wave-like behaviour proportional to $\exp\left[-{\rm i}(\omega t - m\phi)\right]$ for linear perturbations of the whole system, the dispersion relation becomes:

$$\tanh\left\{\frac{2mW^{1/2}}{3}\left[(-Y)^{3/2} - \left(\frac{w_\theta}{\rho} - Y\right)^{3/2}\right]\right\} = W^{1/2}\frac{W_i^{1/2} + W_e^{1/2}}{W + W_i^{1/2} W_e^{1/2}}. \tag{55}$$

Let us notice that the radial width in the cylindrical system of coordinates, w_ϱ is approximately equal to the angular width w_θ in the spherical geometry, so that the above dispersion relation is correct in a cylindrical geometry. Such a dispersion relation for finite beam and plasma flows differs from

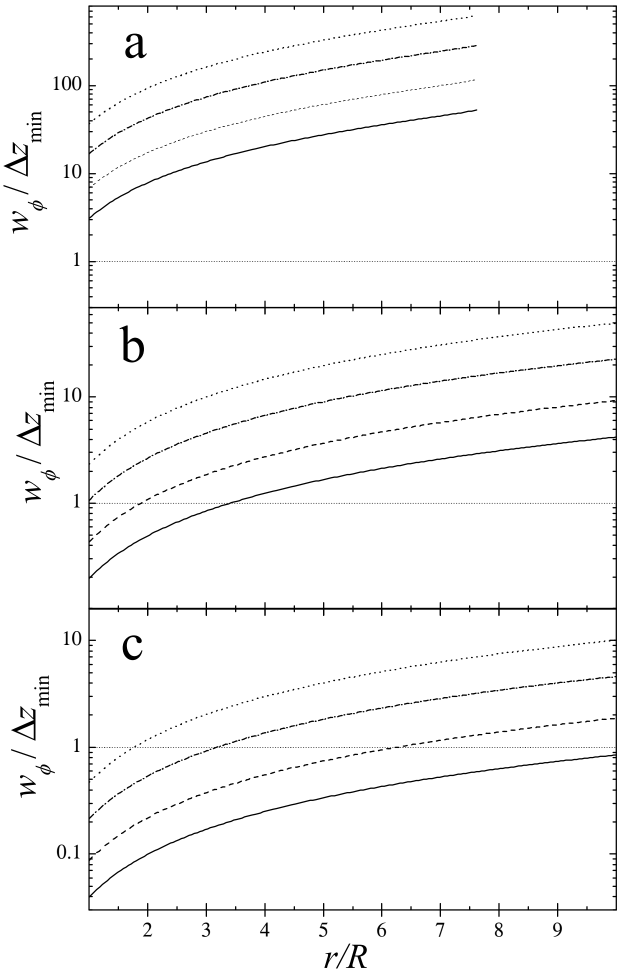

Figure 13. The condition (53) at different distances from the stellar centre. The panels (a), (b) and (c) represent the results of calculations for the sample pulsars with periods equal to 1.6×10^{-3} s, 0.1 s and 1.0977 s (PSR B0943+10), respectively. In each of the panels, solid curves correspond to the observed frequency $\nu = 34$ MHz, dashed curves to $\nu = 111.5$ MHz, dashed-dotted curves to $\nu = 430$ MHz and the dotted curves to $\nu = 1.4$ GHz.

the dispersion relation that characterizes the two-stream instability obtained for infinite and homogeneous beam and plasmas described in a straight geometry, namely $W = 0$. It is modified due to the presence of external media with dielectric constants W_i and W_e. It is also modified due to geometric properties of the flow: more precisely the curvature of the magnetic field, as the radius of curvature ρ of magnetic field lines is involved, the finite width of the beam w_θ and the azimuthal wave-number of the perturbation m. The analysis of this modified dispersion relation in different limits shows that it allows the description of both the radiative (see Goldreich & Keeley (1971) who first described it) and two-stream instabilities, well-known in the context of pulsar physics, but also that there is an unexpected instability: the 'finite beam instability', which even develops for a one-component beam of relativistic mono-energetic particles bounded by external media.

The characteristics of the 'finite beam instability' were obtained in the most general conditions for a beam bounded by identical, or non-identical, external media from the above dispersion relation (Asseo 1995). The case of a beam bounded by identical external media with $W_i = W_e$, is of interest here for an ensemble of beams delineated by the superposition of a strong multipole magnetic field plus a dipole field. In the 'thin' beam case with $Y \gg w_\theta/\rho$, the dispersion relation simplifies to:

$$\left(\frac{W}{W_i}\right)^{1/2} \tanh\left(\frac{1}{{\rm i}\epsilon\sqrt{2}} W^{1/2} Y^{1/2}\right) = 1. \qquad (56)$$

The dependence on the presence of external plasmas appears through W_i. The dependence on the geometric properties of the flow appears through the parameter:

$$\epsilon = \frac{\rho}{m}\frac{1}{w_\theta}. \qquad (57)$$

For the magnetic configuration which includes both dipolar and multipolar magnetic field components, the value of the radius of curvature of magnetic field lines varies with the distance from the stellar surface. Within the gap region from which the beams are issued, the radius of curvature of magnetic field lines is of the order, or even less, than the radius of the star, $\rho \leq R_{\rm s}$. Beyond, in the region where the dipolar magnetic field is dominant, the radius of curvature is approximately $\rho \sim 10^2 R_{\rm s}$, (indeed, $\rho \approx (4r/3\theta) \approx 10^8$ cm at the distance $r = 2R_{\rm s}$). Therefore, the azimuthal wavenumber which corresponds to the resonant frequency at which the instabilities are triggered off, fixed by the relation $m \approx \rho\omega_{\rm R}/c$, slightly varies in the radio emission domain which starts above the gap region (see Asseo 1995). At such resonant frequencies,

$$\epsilon = \frac{\rho}{m}\frac{1}{w_\theta} = \frac{c}{\omega_{\rm R}}\frac{1}{w_\theta} \qquad (58)$$

only depends on the radial extent of the involved annular beam or sub-beams. Numerical estimates with usual parameters for a pulsar with $P = 1$ s show that in the domain of observed radio frequencies $\omega_{\rm R} \leq 1.6 \times 10^9$ Hz and for the radius of curvature of magnetic field lines in the domain $\rho \leq 10^8$ cm, ϵ is smaller than unity.

Above the gap region, but relatively close to it, the ratio of the ring width to the radius of curvature of magnetic field lines is very small, $w_\theta/\rho \leq 2\times10^{-5}$, for values of the radius of curvature in the domain $\rho \leq 10^8$ cm. Thus, we are in the thin beam case, the dispersion relation (55) is valid in its limiting form (equation 56), and the approximation $\tanh\{\ldots\} \approx 1$ is adequate, the parameter ϵ being much smaller than unity. In this case, the dispersion relation (55) simplifies to $W = -W_i$. Such a dispersion relation is adequate to describe a limited region of emission whatever its altitude.

For a one-component beam of relativistic particles with Lorentz factors γ_p, the dielectric constant W is defined as:

$$W = 1 - \frac{\mathcal{P}^2(r)}{Y^2}, \qquad (59)$$

and the dielectric constant W_i of the interior plasma supposed to be at rest is defined as,

$$W_i = 1 - \mathcal{P}_i^2(r)(1 - 2Y). \qquad (60)$$

Here,

$$\mathcal{P}(r) = \frac{\omega_p(r)}{\gamma_p^{3/2} m\Omega_0}, \quad \mathcal{P}_i(r) = \frac{\omega_{pi}(r)}{m\Omega_0}, \qquad (61)$$

whereas $\omega_p(r) = \left[4\pi n_p(r)e^2/m\right]^{1/2}$ and $\omega_{pi}(r) = \left[4\pi n_{pi}(r)e^2/m\right]^{1/2}$, the plasma frequencies in the flowing beam and in the exterior media, respectively, vary along magnetic flux tubes with the corresponding densities. Thus, $\mathcal{P}(r)$ and $\mathcal{P}_i(r)$ depend on the densities in the interior and exterior flux tubes, respectively. Assuming that, as mentioned above, the density within the magnetic flux tube is proportional to the Goldreich & Julian (1969) density,

$$n_p(r) = \kappa n_{\rm GJ}(r), \tag{62}$$

whereas the density in the exterior media $n_{pi}(r)$ is equal to the Goldreich & Julian density,

$$n_{\rm GJ}(r) = \frac{B_{\rm s}}{ecP}\left(\frac{R_{\rm s}}{r}\right)^3 \approx 7\times10^{-2}\frac{B_{\rm s}}{P}\left(\frac{R_{\rm s}}{r}\right)^3 \ [{\rm cm}]^{-3}, \tag{63}$$

we have,

$$\mathcal{P}(r) \approx 1.5\times10^4\sqrt{\kappa\frac{B_{\rm s}}{P}\left(\frac{R_{\rm s}}{r}\right)^3}\frac{1}{\gamma_p^{3/2}m\Omega_0}, \tag{64}$$

$$\mathcal{P}_i(r) \approx 1.5\times10^4\sqrt{\frac{B_{\rm s}}{P}\left(\frac{R_{\rm s}}{r}\right)^3}\frac{1}{m\Omega_0}. \tag{65}$$

Let us note that W_i varies according to the value of $\mathcal{P}_i(r)$ in the emission region, namely:

(i) $W_i \approx 2Y$ at the transition zone located at the distance $r \approx r_{\rm lim}$ where $\mathcal{P}_i(r) \approx 1$.

(ii) $W_i \approx -\mathcal{P}_i^2(r)$ close to the surface of the star where $\mathcal{P}_i(r) \gg 1$, at distances $r < r_{\rm lim}$.

(iii) $W_i \approx 1$ beyond the transition zone where $\mathcal{P}_i(r) \ll 1$, at distances $r > r_{\rm lim}$.

Including a multipolar magnetic field superimposed over the dipolar field and assuming that at the surface of the star the intensity of the multipolar magnetic field is proportional to the strength of the dipole field, $B_{\rm s}^{lm} = (\beta_{\rm s}-1)B_{\rm s}^{\rm d}$ (where β_s has been defined in equation 31), we have for the total field, $B(r) = B_{\rm s}^{\rm d}(R_{\rm s}/r)^3 + (\beta_{\rm s}-1)B_{\rm s}^{\rm d}(R_{\rm s}/r)^{l+2}$. Therefore, the distance $r_{\rm lim}$, at which $\mathcal{P}_i(r) \approx 1$, is not significantly different from the distance $r_{\rm lim}$ obtained in the case where there are no multipolar field components in addition to the dipolar field, as the relative contribution of the multipolar magnetic field, $(\beta_{\rm s}-1)(R_{\rm s}/r)^{l-1}$, is very small. In effect, $r_{\rm lim}$ is simply determined from the relation

$$\mathcal{P}_i(r_{\rm lim}) = xf\left(r_{\rm lim}\right) = 1, \tag{66}$$

where

$$x = 1.5\times10^4\sqrt{\frac{B_{\rm s}^{\rm d}}{P}}\frac{1}{m\Omega_0} \tag{67}$$

and

$$f(r) = \sqrt{\left[1+(\beta_{\rm s}-1)\left(\frac{R_{\rm s}}{r}\right)^{l-1}\right]\left(\frac{R_{\rm s}}{r}\right)^3}. \tag{68}$$

$r_{\rm lim}$ increases with the strength of the total magnetic field but decreases as the pulsar period and the frequency associated with the circulation of relativistic beam particles increase.

In the extreme case of a millisecond pulsar with parameters $P = 0.0016$ s, $B_{\rm s}^{\rm d} = 10^8$ G, $m\Omega_0 = 10^9$ Hz, we obtain $r_{\rm lim} = 2.4\times10^6$ cm. For a 'normal' pulsar with parameters $P = 0.1$ s, $B = 10^{11}$ G, $m\Omega_0 = 10^9$ Hz, we obtain $r_{\rm lim} \approx 6\times10^6$ cm. For a 'slower' pulsar with parameters $P = 1$ s, $B = 10^{11}$ G, $m\Omega_0 = 10^9$ Hz, we obtain $r_{\rm lim} \approx 3\times10^6$ cm. Therefore, whatever the type of pulsar, $r_{\rm lim} \approx$ a few $R_{\rm s}$.

The distance $r_{\rm lim}$ is important in delineating the different regions of instability: below $r_{\rm lim}$ the 'finite beam instability' is dominant whereas beyond $r_{\rm lim}$ either the radiative or the two-stream instabilities prevail. As a matter of fact, the behaviour and growth rate of the 'finite beam instability' is different according to the distance of the considered emission region to the stellar surface. The characteristics of the unstable waves excited trough the 'finite beam instability' – frequency, polarisation, available electromagnetic energy and growth rate – are in agreement with pulsar radio observations (Asseo 1995). Thus, the 'finite beam instability' will initiate the radio emission process in the ensemble of beams with their origin in the gap region, relatively close to the surface of the star. Moreover, such an instability strongly depends on the ratio of densities at the basis of the magnetic tube within and outside the limited beam. As the density of the created pair plasma may vary, an observed apparent motion of the beams around the magnetic axis could be related to variations of the densities within and outside the successive tubes.

4.3 The case of slow pulsars and PSR B$0943+10$

Numerical estimates concerning the above constraint on the spatial extension of the beams, required to ignore azimuthal variations of the perturbations (equation 53), show that in the case of PSR B$0943+10$ this constraint is not uniformly satisfied in the whole region above the gap (see Fig. 13(c)). The distance $r_{\rm 2D}$ from the center of the star beyond which the constraint is satisfied varies with the frequency of observation: as clear from Fig. 13(c), larger distances correspond to lower frequencies. Indeed, $r_{\rm 2D} \approx 2.3\times10^6$ cm for a frequency of observation $\nu = \omega/2\pi \approx 430$ MHz, $r_{\rm 2D} \approx 4.6\times10^6$ cm for $\nu \approx 111.5$ MHz and $r_{\rm 2D} \approx 8.7\times10^6$ cm for $\nu \approx 34$ MHz.

Consequently, between the gap region and the location $r = r_{\rm 2D}$, it is necessary to take into account the 3-dimensional character of the perturbations able to propagate in the system of discrete sub-beams: the density variations in the direction corresponding to the azimuthal ϕ-direction of the spherical geometry, that is to say, in the transverse z-direction of the cylindrical geometry, cannot be further ignored and the ensemble of sub-beams has to be considered as a whole system immersed in 'infinite' exterior media. Thus, an additional systematic azimuthal variation of the perturbations below $r_{\rm 2D}$ will exist and modify the character of perturbations beyond $r_{\rm 2D}$, in the domain where 2-dimensional perturbations are dominant. In fact a coupling of the different perturbed physical quantities is involved as soon as one introduces an azimuthal dependence of the perturbations at relatively small distances from the surface of the star. A thorough treatment including the dependence on the coordinates (r, ϕ, z) of the specified cylindrical geometry of the perturbations is possible as in Asseo et al. (1983), writing the perturbations as of the type:

$$g(z,r)\exp\left[-{\rm i}k_z z\right]\exp\left[-{\rm i}(\omega t - m\phi)\right]. \tag{69}$$

Obviously, the character of the perturbations in the region located beyond r_{2D} has to approach the one described above for fast pulsars, whereas in the region below r_{2D} it is modified by the dependence on the variable z and wave-number k_z. Although we here restrict to a qualitative explanation, and leave exact calculations concerning the character of 3-dimensional perturbations for future work, this suggests that for PSR B0943 + 10, the observed 'rotation', and/or 'drifting', of the emitting columns may be a trace of the initial waves formed in the region below r_{2D} and of their transition towards the above region.

Most of the pulsars which exhibit beautiful drifting subpulses – PSRs 0809 + 74, 0320 + 39, 0820 + 02, 0818 − 13, 1540 − 06 and 0943 + 10 – show periodic drifts (as observed and/or classified by Rankin (1986), see table 2 therein). We notice that all the quoted pulsars have sufficiently long periods to be modelled in analogy of PSR B0943 + 10. This suggests that 'drifting' effects, already known as intrinsically conal phenomena and associated with the circulation of disturbances within the annular polar cap region, could also result from similar perturbations moving within a hollow conical region fragmented into discrete sub-beams. Then, azimuthal widths of the sub-beams will be reflected in the character of unstable excited perturbations.

5 SUMMARY

In this paper we study the complex magnetic topology in the vicinity of neutron stars. We restrict to the case of the aligned rotator, assuming parallel, or anti-parallel, orientation of the rotation and magnetic axes. We assume that the total magnetic field results from the superposition of the global dipolar field and of star-centered multipolar fields of comparable, or even of higher strength. We obtain the following results:

(i) For configurations involving axially symmetric and uniform multipolar magnetic fields it is not possible to obtain small curvature radii of the magnetic field lines, even for multipoles of higher order and strength relative to the dipolar field. Let us recall that according to pulsar polar gap models, curvature radii of the order of the stellar radius are crucial for an efficient pair creation process.

(ii) An interesting consequence of such a magnetic topology is the existence of 'neutral points' and 'neutral lines' above one of the pulsar polar caps. We plan to study implications of such peculiar features of the magnetic field geometry in future works.

(iii) For configurations involving axially symmetric and non-uniform multipolar magnetic fields, the magnetic field structure just above the polar cap is modified in such a way that the pair plasma flow at high altitudes appears as modulated in separate filaments regularly distributed around the outer margin of the open flux tube. Such filaments have their feet in the modified polar cap. They are thin and have finite radial and azimuthal extents. Therefore, the non-uniform pattern of the distribution of curvature radii over the polar cap is reflected in the inhomogeneous distribution of the pair plasma density within the cross-section of the open flux tube at high altitudes.

(iv) For the particular superposition of a dipolar field and a multipolar field of order $l = 20$ and $m = 20$, the magnetic topology causes fragmentation of the pair plasma flow into twenty isolated thin filaments. This resembles the set of twenty sub-beams observed by Deshpande & Rankin (1999, 2001) in PSR B0943 + 10.

(v) Emission in such a system of isolated thin beams, flowing along the curved magnetic field lines, can be described in terms of unstable waves excited by specific instabilities. Relativistic finite beams flowing in the pulsar magnetosphere along a limited fraction of the hollow cone surrounding the magnetic axis can be treated as immersed in exterior media, namely the medium in the closed field line region and the medium within the hollow cone of the open magnetosphere (Asseo 1995). Three different instabilities may develop in such finite beams, depending on the distance to the center of the star: the 'finite beam', radiative and two-stream instabilities. As previously obtained by Asseo (1995), close to the surface of the star the 'finite beam' instability will generate waves whose properties (frequency, polarisation and available electromagnetic energy) are in agreement with the observed pulsar radio emission.

(vi) We check that the conditions for such a treatment are relevant for the configuration of discrete sub-beams that may exist in millisecond and fast pulsars. They are also relevant for slower pulsars, like PSR B0943 + 10, beyond some distance from the gap region. On the other hand, closer to the gap of such a slow pulsar, the radial and azimuthal variations of the flowing sub-beams cannot be separated; the system of sub-beams has to be treated as a whole; the 3-dimensional character of the perturbations will introduce some 'drift' of the emitted waves; such a 'drift' effect will be transferred to high altitudes due to the necessary continuity between the vicinity of the gap and the farther region. In this way, the continuity of the flow all along magnetic flux tubes and of the perturbations carried by it, accounts for the 'drifting' character of the subpulses observed in pulsar radio profiles.

6 ACKNOWLEDGMENTS

It is a pleasure to thank our referee for reading carefully our manuscript and suggesting changes which have been fruitful to improve our paper. D.K. would like to thank G. Melikidze, V. Usov and J. Gil for fruitful discussions. D.K. is also very grateful to the scientific staff of the Centre de Physique Théorique (CNRS UMR 7644) for hospitality during his stay at Ecole Polytechnique.

REFERENCES

Abramowitz M., Stegun I. A., 1965, Handbook of Mathematical Functions. Dover Publications, Inc., New York
Anderson J. L., Cohen J. M., 1970, Ap&SS, 9, 146
Arons J., Scharlemann E. T., 1979, ApJ, 231, 854
Arons J., 1993, ApJ, 408, 160
Asseo E., 1995, MNRAS, 276, 74
Asseo E., Pellat R., Sol H., 1983, ApJ, 266, 201
Asseo E., Melikidze G. I., 1998, MNRAS, 301, 59
Barnard J. J., Arons J., 1982, ApJ, 254, 713
Blandford R. D., Applegate J. H., Hernquist J., 1983, MNRAS, 204, 1025
Chen K., Ruderman M. A., 1993, ApJ, 402, 264
Cheng K. S., Zhang L., 1999, ApJ, 515, 337
Daugherty J., Harding A. K., 1983, ApJ, 273, 761

Davies J. G., Lyne A. G., Graham-Smith F., Izvekova V. A., Kuzmin A. D., Shitov Yu. P., 1984, MNRAS, 211, 57
Deshpande A. A., Rankin J. M., 1999, ApJ, 524, 1008
Deshpande A. A., Rankin J. M., 2001, MNRAS, 322, 438
Forsythe G., Malcolm M., Moler C., 1977, Computer Methods for Mathematical Computations. Prentice-Hall
Gil J. A., 1985, A&A, 143, 443
Gil J. A., Mitra D., 2001, ApJ, 550, 383
Goldreich P., Julian H., 1969, ApJ, 157, 869
Goldreich P., Keeley D. A., 1971, ApJ, 170, 463
Jackson J. D., 1975, Classical Electrodynamics. Wiley Interscience, New York
Krolik J. H., 1991, ApJ, 373, L69
Kuzmin A. D., 1992, in Hankins T. H., Rankin J. M., Gil J. A., eds., IAU Colloq. 128: Magnetospheric Structure and Emission Mechanisms of Radio Pulsars (Zielona Góra, Poland), p. 2
Melikidze G. I., Gil J. A., Pataraya A. D., 2000, ApJ, 544, 1081
Mitra D., Konar S., Bhattacharya D., 1999, MNRAS, 307, 459
Muslimov A. G., Tsygan A. I., 1986, AZh, 63, 958
Muslimov A. G., Tsygan A. I., 1992, MNRAS, 255, 61
Page D., Sarmiento A., 1995, ApJ, 442, 273
Page D., Sarmiento A., 1996, ApJ, 473, 1067
Radhakrishnan V., Cooke D. J., 1969, ApL, 3, 225
Rankin J. M., 1986, ApJ, 301, 90
Ruderman M. A., Sutherland P. G., 1975, ApJ, 196, 51
Ruderman M. A., 1991a, ApJ, 366, 261
Ruderman M. A., 1991b, ApJ, 382, 576
Ruderman M. A., 1991c, ApJ, 382, 587
Sturrock P. A., 1971, ApJ, 164, 529
Ursov V. N., Usov V. V., 1988, Ap&SS, 140, 325
Usov V. V., 1987, ApJ, 320, 333
Young M. D., Manchester R. N., Johnson S., 1999, 400, 848
Xu R. X., Qiao G. J., Zhang B., 1999, ApJ, 515, 398